Medical Image Analysis 75 (2022) 102300

Contents lists available at ScienceDirect

Medical Image Analysis

journal homepage: www.elsevier.com/locate/media

A new baseline for retinal vessel segmentation: Numerical identification and correction of methodological inconsistencies affecting 100+ papers

György Kovács [a,*], Attila Fazekas [b]

[a] Analytical Minds Ltd., Árpád street 5, Beregsurány 4933, Hungary
[b] University of Debrecen, Faculty of Informatics, P.O.BOX 400, Debrecen 4002, Hungary

ARTICLE INFO

Article history:
Received 21 March 2021
Revised 20 September 2021
Accepted 4 November 2021
Available online 13 November 2021

Keywords:
Vessel segmentation
Numerical analysis
Accuracy
Retina

ABSTRACT

In the last 15 years, the segmentation of vessels in retinal images has become an intensively researched problem in medical imaging, with hundreds of algorithms published. One of the *de facto* benchmarking data sets of vessel segmentation techniques is the DRIVE data set. Since DRIVE contains a predefined split of training and test images, the published performance results of the various segmentation techniques should provide a reliable ranking of the algorithms. Including more than 100 papers in the study, we performed a detailed numerical analysis of the coherence of the published performance scores. We found inconsistencies in the reported scores related to the use of the field of view (FoV), which has a significant impact on the performance scores. We attempted to eliminate the biases using numerical techniques to provide a more realistic picture of the state of the art. Based on the results, we have formulated several findings, most notably: despite the well-defined test set of DRIVE, most rankings in published papers are based on non-comparable figures; in contrast to the near-perfect accuracy scores reported in the literature, the highest accuracy score achieved to date is 0.9582 in the FoV region, which is 1% higher than that of human annotators. The methods we have developed for identifying and eliminating the evaluation biases can be easily applied to other domains where similar problems may arise.

1. Introduction

Retinal images provide a noninvasive way to detect and monitor various conditions and diseases of the eye and body, such as diabetes-related retinopathies, macular degeneration, glaucoma and hypertension (Abramoff et al., 2010). Consequently, the computer-aided (semi-)automatic analysis and screening of retinal images has become a highly popular field of study in medical imaging, with thousands of papers and algorithms focusing on various anatomical parts and degenerations observable in retinal images (Abramoff et al., 2010; Trucco et al., 2019). The popularity of the field can be illustrated by the numerous challenges on the segmentation and grading of retinal images in recent years, organized by data science competition platforms (such as the Diabetic Retinopathy Challenge on Kaggle[1]), and as special tracks of corresponding conferences (like "IDRiD: Diabetic Retinopathy Segmentation and Grading Challenge" (Porwal et al., 2020)).

A particularly popular problem in retinal image analysis is the segmentation of retinal vessels (illustrated in Fig. 1). The importance of the problem is threefold. On the one hand, the characteristics of the vasculature can aid the early detection of diseases like hypertension (lui Cheung et al., 2012). On the other hand, the removal of vessels usually precedes the detection of other anatomical parts. For example, the high curvature and junction points of thin vessels have similar visual features to microaneurysms (Long et al., 2020), consequently, the segmentation of the vasculature can indirectly aid the detection of mycroaneurysms. Finally, the segmented vasculature may serve as a guide for locating other anatomical parts, such as the macula (Yu et al., 2014).

In competitive research fields, where the primary goal is to find the most accurate solution to a problem, the proper comparison of algorithms is crucial. Comparability requires the coordination of evaluation data sets and methodologies that fit the purpose of the problem. As pointed out recently (Maier-Hein et al., 2018), even the grand challenges of recent years tend not to produce robust and reliable rankings. Therefore, the study of evaluations in active

* Corresponding author.
E-mail addresses: gyuriofkovacs@gmail.com (G. Kovács), attila.fazekas@inf.unideb.hu (A. Fazekas).

[1] https://www.kaggle.com/c/diabetic-retinopathy-detection.

https://doi.org/10.1016/j.media.2021.102300
1361-8415/

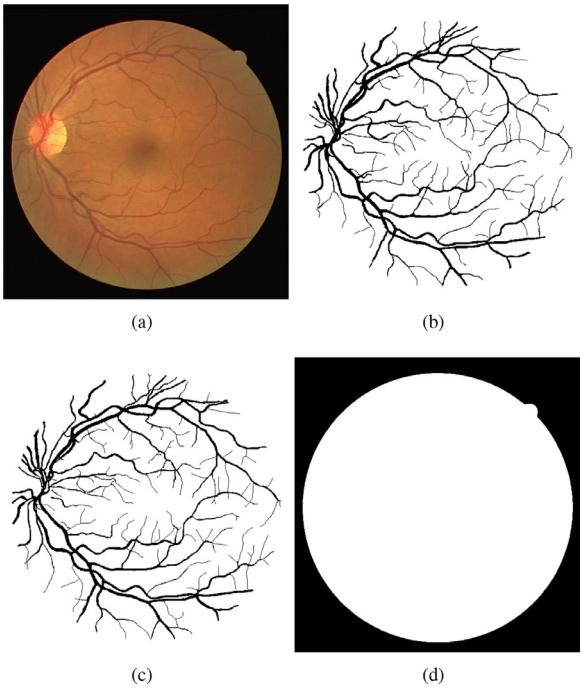

Fig. 1. The "01" entry of the test set in the DRIVE database: retinal image (a); manual segmentation #1 (with inverted intensities for visibility) (b); manual segmentation #2 (inverted) (c); field-of-view (FoV) mask, covering the meaningful image content (d).

research areas such as retinal vessel segmentation is desirable to understand the state of the art.

In a self-organised fashion, three data sets have emerged as the *de facto* standard for the evaluation of vessel segmentation: DRIVE (Niemeijer et al., 2004), STARE (Hoover et al., 2000) and HRF (Budai et al., 2013). Of these, HRF is relatively new, and many classical algorithms have not yet been evaluated on it. STARE is not split into training and test sets, and the ambiguities of cross-validation lead to uncertain and hardly comparable results. In contrast, DRIVE eliminates many ambiguities of the evaluation by providing a predefined split of training and test images. Because of their long history, DRIVE and STARE continue to be the primary data sets for evaluation in recent work (Jin et al., 2019; Xiuqin et al., 2019), and due to predefined test set in DRIVE, the results obtained on DRIVE are generally accepted as comparable, which is reflected in the numerous rankings in the papers showing the merits of the newly proposed algorithms. The most commonly reported performance measures are the accuracy, sensitivity and specificity of the segmentation.

In a previous paper of ours (Kovács and Hajdu, 2016), we briefly pointed out that despite the predefined training and test sets in DRIVE, there is a potential methodological flaw in the evaluations, invalidating many rankings and comparisons in the literature. Namely, textual evidence suggests that some authors compute the performance scores in the field-of-view (FoV) region (Fig.), while others compute the scores for all pixels of the images (the entire rectangular area including the black surroundings of the FoV in Fig.). This minor difference affects the accuracy and specificity scores enormously. Due to the continued interest in this topic, we found it worthwhile to investigate the evaluation methodologies and their impact on comparability in detail. In this paper, we carry out a detailed numerical analysis of the phenomenon including more than 100 papers from the literature. In order to work with a sufficiently large population and eliminate the ambiguity of cross-validation, we investigate the accuracy, sensitivity and specificity scores reported for the test set of DRIVE. Our main contributions to the field can be summarized as follows:

1. We introduce numerical approaches to uncover some details of the evaluation methodologies used in 100 relevant papers. The results provide inevitable evidence for two main types of methodologies with non-comparable performance scores: evaluation under the FoV mask and evaluation using all pixels.
2. We attempt to eliminate the biases using numerical techniques to produce a more realistic ranking of algorithms.
3. Our results confirm that most rankings in the literature are based on non-comparable figures, the state of the art performance cannot be deduced without the numerical inference and categorization of evaluation methodologies and adjustments of published figures.
4. The techniques we introduce can be transferred to other areas where the identified methodological flaw is potentially present.
5. According to our best knowledge, this is the first study investigating the coherence of a subfield of medical image analysis by numerical techniques.
6. For complete reproducibility, the raw data, the implementation of the analysis and the results are shared in the GitHub repository https://github.com/gykovacs/retina_vessel_segmentation.

The paper is organized as follows. In Section 2, we describe the details of the data set DRIVE and formulate the problem we address by providing textual evidence for its existence. In Section 3, we introduce the numerical methods and present the raw results. Based on the findings of the numerical analysis, we discuss the state of the art in Section 4. Finally, we summarize the paper and draw conclusions in Section 5.

2. Problem formulation

In this section, we describe the main characteristics of the data set DRIVE, the performance scores, and we also discuss and illustrate the root cause of the problem we address.

2.1. The DRIVE data set

The Digital Retinal Images for Vessel Extraction (DRIVE) data set (Niemeijer et al., 2004) contains 20 training and 20 test entries. Images were captured with a Canon CR5 non-mydriatic 3CCD camera with a 45 $^\circ$ field of view and cropped to 584 $\times$ 565 pixels. Each training entry consists of a retinal image, a binary annotation of vessels (by annotator #1), and a binary mask of the Field of View (FoV) indicating the useful image content. The FoV masks cover 69% of the rectangular images. Each test entry includes an additional manual segmentation by annotator #2, enabling the evaluation of human annotators as a baseline. A complete entry from the test set is visualized in Fig. 1.

2.2. Performance metrics

There are numerous metrics in the literature to characterize the performance of image segmentation algorithms. In retinal vessel segmentation, most authors report some metrics of binary classification performance at the pixel level. Particularly, a segmentation is compared to the ground truth image to determine the number of

- true positives (tp) - correctly identified vessel pixels;
- true negatives (tn) - correctly identified non-vessel pixels;
- false positives (fp) - non-vessel pixels identified as vessel;
- false negatives (fn) - vessel pixels identified as non-vessel;

and introducing $p = tp + fn$ and $n = tn + fp$ for the total number of vessel and non-vessel pixels, respectively, the scores

- accuracy ($acc = (tp + tn)/(p + n)$) - the proportion of all correctly identified pixels to all pixels;
- sensitivity ($sens = tp/p$) - the proportion of correctly identified vessel pixels to all vessel pixels;
- specificity ($spec = tn/n$) - the proportion of correctly identified non-vessel pixels to all non-vessel pixels

are reported at the image level or averaged on all test images. Some authors report the complements of the *sens* and *spec* scores known as false negative (1 - *sens*) and false positive (1 - *spec*) rates, respectively. We highlight that vessel segmentation as a binary classification problem is highly imbalanced, i.e., the number of vessel pixels in the FoV region is 15% of the number of non-vessel pixels, leading to high absolute accuracy and specificity scores: a 0.1% improvement in accuracy implies the correct segmentation of about 250 additional pixels, which is 1% of the size of the vasculature.

Since the goal is usually to maximize both sensitivity and specificity (and thus maximize accuracy), some authors report other composite measures of sensitivity and specificity, such as the F_1-score (the harmonic mean of *sens* and *spec*) or the AUC score (Hanley and Mcneil, 1982), however, these scores are reported too infrequently to rely a comprehensive analysis on them. Therefore, in the remainder of the paper, we focus on the *acc*, *sens* and *spec* scores.

2.3. The source of ambiguity

Although DRIVE specifies dedicated training and test sets, there is some ambiguity regarding the comparability of published performance scores. For example, one of the earliest papers (Staal et al., 2004) explicitly states:

> "Since the dark background outside the FOV is easily extracted, in this paper all experiments are done on the FOV only."

On the other hand, (Villalobos-Castaldi et al., 2010) says:

> "Based on a total of 329,960 pixels contained in a fundus image of size 565 × 584 pixels, it is possible to obtain the TP, TN, FP, and FN quantities of the segmented image."

Finally, the authors of (Yu et al., 2012) explicitly state that

> "It is mentionable that the accuracy and FPR [false positive rate] measures in Jiang (Jiang and Mojon, 2003), Martinez-Perez (Martinez-Perez et al., 2007), and Miri's (Miri and Mahlooji-far, 2010) methods were calculated in the complete image instead of the FOV."

Even this handful of quotations suggests that some authors evaluate performance only in the area covered by the FoV mask, while others use all pixels of the images. The pixels outside the FoV are usually non-vessel pixels accounting for about 31% of all pixels in the images. If they are treated as true negatives, the accuracy and specificity increases tremendously. To illustrate the magnitude of this effect, we evaluate the segmentation of annotator #2 against annotation #1 (as ground truth) under the FoV mask and including all pixels of the images. With the FoV mask, $acc = 0.9473$, $sens = 0.7760$ and $spec = 0.9725$, but using all pixels, $acc = 0.9636$, $sens = 0.7756$ and $spec = 0.9818$. Omitting the FoV mask increased the *acc* and *spec* values by more than 1.5% and 1%, respectively. The slight change in sensitivity is due to an average of 15 vessel pixels in the annotations #1 being outside the FoV. Since many authors report 0.1% improvements in accuracy, the variation in the region used for evaluation can cause an enormous bias when algorithms are compared and ranked.

In the rest of the paper, we develop numerical techniques to test the consistency of the published figures with the hypotheses that the authors either evaluated under the FoV mask or used all pixels of the images.

2.4. The need for the numerical analysis

We attempt to investigate the evaluation methodology of dozens of complex image processing pipelines. Collecting original implementations covering 15 years of technological development seems to be unmanagable. On the other hand, reimplementations of the algorithms are unlikely to reproduce the exact figures shared by the authors as all details of complex image processing pipelines are rarely shared due to length limitations. To avoid further bias and to treat all papers similarly and equally, we decided to base the study only on the shared performance scores. In order to draw conclusions without statistical uncertainties, we decided to rely on numerical analysis to reveal some details of the evaluation methodologies used by the authors.

3. Methods and raw results

In this section, the steps of the numerical analysis are described and the corresponding results are reported. The raw results are turned into insights and discussed in detail in Section 4. We introduce two special notations: The mean of a set of figures is denoted by an overline (such as $\overline{acc}$ standing for the mean of a set of accuracy scores), and asterisk indicates exact values with no uncertainty (such as tp^* standing for the exact number of true positives) that can either be extracted from the publicly available data set or denote unknown but exact values extracted by the authors to calculate the performance scores they reported.

3.1. The papers and algorithms involved

To select a sufficiently large, influential and comprehensive population of algorithms and reported performance scores without subjective bias, we applied the following strategy. We searched for the term *retinal vessel segmentation* in three of the largest scientific publication databases (*Elsevier ScienceDirect, IEEE Xplore* and *ACM Digital Library*) and recursively added the most cited ones with all algorithms referenced in them until we reached 90 papers. Finally, 10 recent papers, mainly based on deep learning have been added to represent the latest trends. To maintain quality and achieve the goals of our study, papers that met any of the following exclusion criteria were omitted in the selection process:

- not sharing *acc*, *sens* and *spec* scores for DRIVE;
- early papers of authors with multiple papers in the field;
- being published only on preprint servers;
- not reporting performance scores to at least 3 decimal places (rounding of the scores to 2 decimal places introduces larger uncertainty than the size of the bias we investigate).

A summary of the papers in Table 1 shows some interesting insights into the evaluation methodologies. Authors rarely phrase explicitly the region they use for evaluation, and when it is shared, a mixture of the two edge cases can be observed: the use of the FoV, and evaluation on all pixels. When the region of evaluation is not shared, one can still observe the two accuracy scores 0.9473 and 0.9637 for annotator #2 (the scores we calculated in Subsection 2.3 under the FoV and using all pixels, repsectively). Finally, a slight variation can be observed in the scores being close to the one computed under the FoV (0.9473). This suggests that custom adjustments to the FoV may also have occured, but there is no textual evidence or indication of the nature of these adjustments.

Table 1
A summary of the papers included in the study, with columns as follows. "Rank": the rank based on the published accuracy scores; "Key": reference to the paper; "$\overline{acc}$": the published accuracy score; "Num. image level": the number of image level figures shared by the authors; "Num. aggregated": the number of aggregated figures shared by the authors; "Annotator #2 acc.": accuracy score of annotator #2; "Region of eval.": the region of evaluation explicitly phrased by authors, 'F' for FoV, 'a' for all pixels, empty when it is not phrased explicitly; "Decimal places": the number of decimal places to which the figures are reported; "Citations": the number of citations at the time of writing this paper.

Rank	Key	$\overline{acc}$	Num. image level	Num. aggre-gated	Annotator #2 acc.	Region of eval.	Decimal places	Citations	Rank	Key	$\overline{acc}$	Num. image level	Num. aggre-gated	Annotator #2 acc.	Region of eval.	Decimal places	Citations
1	Jebaseeli et al. (2019)	0.9898		1		F	4	6	51	Meng et al. (2015)	0.9529	20	1	0.9470	F	4	13
2	Hassanien (2018)	0.9793	20	1			4	24	52	Li et al. (2016)	0.9527	2	3	0.9472		4	306
3	Wang et al. (2015)	0.9767	20	9	0.9464	F	4	274	53	Imani et al. (2015)	0.9523	20	5	0.9473		4	84
4	Villalobos-Castaldi et al. (2010)	0.9759		1	0.9473	a	4	70	54	Singh and Srivastava (2016)	0.9522	20	1		a	4	75
5	Memari et al. (2017)	0.9722		3	0.9464		4	23	55	Mo and Zhang (2017)	0.9521	2	3			4	68
6	Park et al. (2020)	0.9706		1			4	2	56	Isavand Rahmani et al. (2020)	0.9521		1			4	0
7	Jiang et al. (2019)	0.9706		9	0.9637		4	9	57	Dash et al. (2020)	0.952	20	1			3	0
8	Atli and Gedik (2021)	0.9689		2	0.9637		4	3	58	Chalakkal and Abdulla (2017)	0.9518		1			4	12
9	Moghimirad et al. (2011)	0.9659	4	1	0.9473	F	4	44	59	Singh and Srivastava (2017)	0.9513	20	1		a	4	3
10	Xiuqin et al. (2019)	0.9650		1			4	12	60	Mapayi et al. (2015)	0.9511		6	0.9473		4	50
11	Escorcia-Gutierrez et al. (2020)	0.964	20	1			3	0	61	Zhang and Chung (2018)	0.9504		1	0.9472		4	53
12	Sreejini and Govindan (2015)	0.9633		1	0.9470		4	47	62	Bharkad (2017)	0.9503	20	1			4	3
13	Saleh et al. (2011)	0.9630		2	0.9473		4	68	63	Barkana et al. (2017)	0.9502	4	4	0.9470	F	4	72
14	Kumar et al. (2016)	0.9626		1			4	28	64	Khan et al. (2016)	0.9501	20	1	0.9473		4	18
15	Wankhede and Khanchandani (2015)	0.9626		1	0.9473	a	4	19	65	Song and Lee (2017)	0.9499		1	0.9473		4	12
16	Pandey et al. (2017)	0.9623		1			4	24	66	Kovács and Hajdu (2016)	0.9494		5	0.9473	F	4	36
17	Narkthewan and Maneerat (2019)	0.9617	20	1			4	2	67	Roychowdhury et al. (2015)	0.9494		1			4	153
18	Waheed et al. (2015)	0.9616	20	1			4	23	68	Brancati et al. (2018)	0.949		5	0.947	F	3	0
19	Xiang et al. (2014)	0.9613		1	0.9612		4	7	69	Nazari and Pourghassem (2013)	0.9481		2	0.9470		4	12
20	Alom et al. (2019)	0.9613		5			4	46	70	Kaur and Mittal (2017)	0.9480		1			4	12
21	Tang et al. (2017)	0.9611	20	1	0.9470		4	6	71	Palanivel et al. (2020)	0.9480		4	0.9470		4	1

(*continued on next page*)

Table 1 (*continued*)

22	Samuel and Veeramalai (2019)	0.9609		4	0.9470		4	14	72	Fraz et al. (2012c)	0.9480	2	3	0.9464	F	4	493
23	Tamim et al. (2020)	0.9607	20	1			4	1	73	Shah et al. (2017)	0.9479		1	0.9473		4	18
24	Zhu et al. (2017)	0.9607	20	9			4	92	74	Zhang et al. (2016)	0.9476		2	0.9472	F	4	171
25	Thangaraj et al. (2018)	0.9606	20	1			4	16	75	Shukla et al. (2020)	0.9476		1	0.9473		4	3
26	Lupascu and Tegolo (2016)	0.9606	40	2	0.9473		4	1	76	Cheng et al. (2014)	0.9474		6	0.9470		4	80
27	Fan et al. (2017)	0.960		2			3	7	77	Zhou et al. (2017)	0.9469		5	0.9473	F	4	33
28	Lupaşcu et al. (2010)	0.9597	7	1	0.9473		4	329	78	Melinscak et al. (2015)	0.9466		1			4	118
29	Ricci and Perfetti (2007)	0.9595	2	1	0.9473	F	4	769	79	Mendonca and Campilho (2006)	0.9463		2	0.9473	F	4	983
30	Wu et al. (2020)	0.9582		3			4	9	80	Rezaee et al. (2017)	0.9463		1	0.9473		4	34
31	Fathi and Naghsh-Nilchi (2013)	0.9581	20	1			4	95	81	Rahebi and Hardala (2014)	0.9461	20	1			4	38
32	Dash and Bhoi (2018)	0.957	20	1			3	14	82	Miri and Mahloojifar (2010)	0.9458		1			4	291
33	Budai et al. (2013)	0.957		1	0.947		3	207	83	Strisciuglio et al. (2016)	0.9454		5			4	64
34	Noh et al. (2019)	0.9569		1	0.9472		4	18	84	Marin et al. (2011)	0.9452	20	1		F	4	906
35	Soomro et al. (2019)	0.956		1			3	17	85	Adapa et al. (2020)	0.9450	20	1			4	4
36	Frucci et al. (2017)	0.956		1			3	3	86	Javidi et al. (2017)	0.9450		1	0.9473	F	4	46
37	Frucci et al. (2016)	0.955	20	1			3	27	87	Azzopardi et al. (2015)	0.9442		3			4	445
38	Saroj et al. (2020)	0.9544	20	1			4	1	88	Strisciuglio et al. (2015)	0.9442		1			4	25
39	Yan et al. (2018)	0.9542		2	0.9472		4	92	89	Staal et al. (2004)	0.9441		1	0.9473	F	4	2830
40	Zhao et al. (2015b)	0.954		5	0.947		3	246	90	You et al. (2011)	0.9434		1	0.9473	F	4	325
41	Na et al. (2018)	0.954		1	0.947		3	6	91	Soomro et al. (2017)	0.9432		1			4	21
42	Panda et al. (2016)	0.9539		4	0.9470	a	4	32	92	Kumar et al. (2020)	0.9432	20	1	0.9473	F	4	0
43	GeethaRamani and Bal/an (2016)	0.9536	20	1	0.9470		4	77	93	Fraz et al. (2012a)	0.9430	2	11	0.9473	F	4	294
44	Liskowski and Krawiec (2016)	0.9535		12	0.9473	F	4	492	94	Dai et al. (2015)	0.9418		1			4	41
45	Soomro et al. (2018)	0.9534		4			4	45	95	Anzalone et al. (2008)	0.9418		1	0.9473	F	4	57
46	Dasgupta and Singh (2017)	0.9533		1			4	133	96	Dizdaroglu et al. (2012)	0.9412		2			4	25
47	Ngo and Han (2017)	0.9533		1			4	19	97	Salazar et al. (2014)	0.9412		1	0.9473	F	4	222
48	Hu et al. (2018)	0.9533		4	0.9470	F	4	87	98	Emary et al. (2014)	0.939	20	1			3	26
49	Yang et al. (2020)	0.9532		4			4	0	99	Zhang et al. (2010)	0.9382		1	0.9473	F	4	530
50	Zhao et al. (2015a)	0.953		10	0.947		3	91	100	Odstrcilik et al. (2013)	0.9340	20	1	0.9473	a	4	266

3.2. Overview of the numerical analysis

The analysis is based on the interdependence of the scores *acc*, *sens* and *spec*. Particularly, these scores cannot take arbitrary values: they are linear functions of the four unknowns tp, tn, fp and fn, which need to sum up to the number of positive (vessel) $p = tp + fn$ and negative (non-vessel) $n = tn + fp$ pixels, while $p + n$ needs to match the size of the FoV mask or the size of the image. Consequently, the reported values of a triplet of *acc*, *sens* and *spec* together with the exact number of positive and negative pixels in the images must satisfy certain conditions. In the rest of the section, this idea is developed further to deal with the numerical uncertainties of rounding and averaging, and to allow inferences to be made about the evaluation methodologies.

3.3. Image level analysis

Some authors have reported the *acc*, *sens* and *spec* scores at the image level. In this subsection, we develop a consistency test to decide whether the image level scores were computed in the FoV region or using all pixels of the images.

3.3.1. The image level consistency test

For each image, the true positives (tp^*) and true negatives (tn^*) calculated by the authors must satisfy the following inequalities by definition:

$$sens - \epsilon \le \frac{tp^*}{p^*} \le sens + \epsilon, \tag{1}$$

$$spec - \epsilon \le \frac{tn^*}{n^*} \le spec + \epsilon, \tag{2}$$

$$acc - \epsilon \le \frac{tp^* + tn^*}{p^* + n^*} \le acc + \epsilon, \tag{3}$$

$$0 \le tp^* \le p^*, \quad 0 \le tn^* \le n^*, \tag{4}$$

where the total number of positive p^* (vessel) and negative n^* (non-vessel) pixels can be determined given the publicly available images, and ϵ denotes the numerical uncertainty of the reported figures. The setting $\epsilon = 10^{-k}/2$ is the maximum numerical uncertainty when the figures reported to k decimal places are subject to rounding, and $\epsilon = 10^{-k}$ is the maximum uncertainty when truncation or ceiling to k decimal places is assumed.

Eliminating tp^* and tn^* from the inequalities gives 6 conditions that must hold for a given triplet of *acc*, *sens* and *spec* scores, regardless of the actual values of tp^* and tn^*:

$$\begin{aligned}
&0 \ge n^*(acc - spec) + p^*(acc - sens) - 2\epsilon(p^* + n^*),\\
&0 \le n^*(acc - spec) + p^*(acc - sens) + 2\epsilon(p^* + n^*),\\
&0 \ge p^*(sens - \epsilon - 1), \quad 0 \le p^*(sens + \epsilon),\\
&0 \ge n^*(spec - \epsilon - 1), \quad 0 \le n^*(spec + \epsilon).
\end{aligned} \tag{5}$$

The conditions (5) allow us to test the consistency of a certain triplet of *acc*, *sens* and *spec* reported for an image with p^* positives and n^* negatives, with ϵ numerical uncertainty. Since we are concerned about two cases (evaluation using the FoV mask or all pixels), one can extract the total number of positives and negatives with and without the FoV and test whether the conditions for either hypothesis are satisfied. For example, treating annotation #1 as ground truth and annotation #2 as a segmentation for the test image in Fig. 1, the rounded performance scores with the FoV mask are $acc = 0.9492$, $sens = 0.7965$, $spec = 0.9722$. In the FoV region, $p^* = 29412$ and $n^* = 194965$, and substituting these figures into the inequalities (5), all conditions are satisfied. On the other hand, including all pixels of the images, $p^* = 29440$ and $n^* = 300520$, and with this substitution the conditions fail.

The conditions (5) are sharp in the sense that if the assumptions on p^* and n^* are correct, then the conditions must hold; if the assumptions on p^* and n^* are sufficiently far the figures used to compute the scores *acc*, *sens* and *spec*, then the test fails. However, due to the numerical uncertainty, scores computed in regions slightly different from the assumptions might also satisfy the conditions (5). This phenomenon is examined in the next subsection.

3.3.2. Sensitivity of the image level consistency test

To quantitatively characterize the sensitivity of the test to changes in the region of evaluation, we carried out a simulation treating annotation #1 as ground truth and annotation #2 as segmentation for all 20 images in the DRIVE test set. The FoV masks were gradually dilated to cover the images; for each mask size, the performance scores were calculated and rounded to 3 and 4 digits; and the tests derived in Subsection 3.3.1 were applied to the scores to check whether they were computed under the original FoV masks or using all pixels of the images. The percentages of image level scores passing the tests at certain mask sizes are plotted in Fig. 2 along with the average accuracy to illustrate the bias caused by the adjustment of evaluation region. The first thing to observe is that varying the size of the evaluation region has a remarkable effect on the accuracy scores. However, when the performance scores are rounded to 4 digits, a deviation as little as 1% from the assumed region makes the test fail on more than 50% of the 20 test images, as can be seen by the steep drop in the corresponding dashed lines around the size of the official FoVs (69% of the image size) and at 100% of the image size. The increased uncertainty of rounding to 3 digits widens the acceptance window (solid lines) and about 50% of the scores pass despite a 15% change in the size of the evaluation region. However, the passing rate drops to about 5% at the opposite assumptions, indicating that the two edge cases can still be distinguished by the test. The analysis suggests that *the consistency test is able to distinguish the cases where the official (or slightly differing) FoV masks were used from those cases when all (or almost all) pixels of the images were included in the evaluation.*

3.3.3. Image level results

The image level consistency test was applied to all image level figures shared by 36 authors. To tolerate possible typos in the published figures and minor deviations from the exact assumptions, the image level results are aggregated according to the following permissive rule. If the use of the FoV (all pixels) is confirmed by the majority of the image level scores shared in a paper, the published scores are accepted to be calculated under the FoV (all pixels). If none of the assumptions are confirmed by the majority of the image level scores passing, all results of the paper are marked as *outliers* in terms of evaluation: in these cases we can state with certainty that the authors evaluated in an unknown way.

The results are summarized in Table 2 and plotted in Fig. 3 in the accuracy-specificity plane. Surprisingly, 20 out of the 36 papers with image level scores turned out to be outliers. The ranking in Table 2 shows that almost all papers where the use of all pixels was accepted outperform those evaluating under the FoV mask, clearly showing the expected skew in the evaluations. A similar pattern can be seen in Fig. 3: the scores where the use of the FoV mask was accepted tend to have lower accuracy and specificity scores than those where the use of all pixels was confirmed.

3.4. The analysis of aggregated figures

Most authors report only the averages of image level performance scores. In this subsection, we develop consistency tests to take into consideration the numerical uncertainty caused by the averaging.

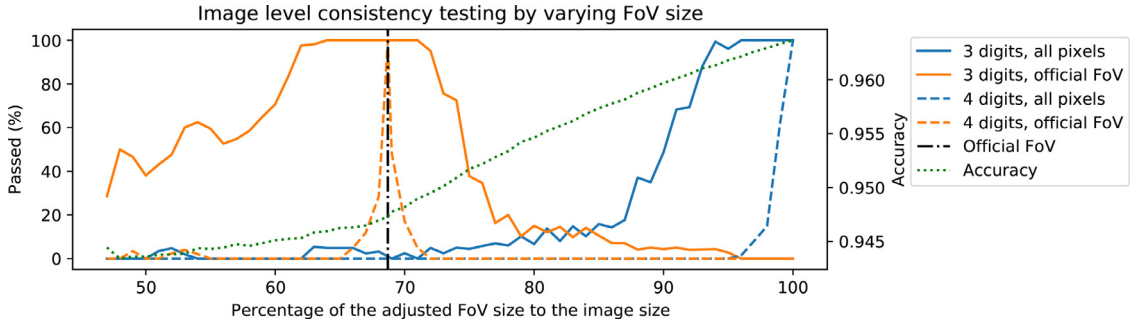

Fig. 2. The percentage of image level scores passing the consistency tests with the two assumptions when the region of evaluation and the rounding of performance scores is varied.

Table 2
Results of the image level consistency tests: the percentages indicate the fraction of image level scores passing the consistency test with a particular assumption on the region of evaluation.

Key	$\overline{acc}$	$\overline{sens}$	$\overline{spec}$	Decimal places	Num. image level fig.	% passed assum. FoV	% passed assum. all pixels	Decision
Hassanien (2018)	0.9793	0.8981	0.9883	4	20	0	5	outlier
Wang et al. (2015)	0.9767	0.8173	0.9733	4	20	0	0	outlier
Moghimirad et al. (2011)	0.9659	0.7852	0.9935	4	4	25	25	outlier
Escorcia-Gutierrez et al. (2020)	0.9640	0.6170	0.9980	3	20	0	0	outlier
Narkthewan and Maneerat (2019)	0.9617	0.6392	0.9920	4	20	0	5	outlier
Waheed et al. (2015)	0.9616	0.7937	0.9779	4	20	0	90	all pixels
Tang et al. (2017)	0.9611	0.8174	0.9747	4	20	0	10	outlier
Tamim et al. (2020)	0.9607	0.7542	0.9843	4	20	0	0	outlier
Zhu et al. (2017)	0.9607	0.7140	0.9868	4	20	0	0	outlier
Thangaraj et al. (2018)	0.9606	0.8014	0.9753	4	20	0	10	outlier
Lupascu and Tegolo (2016)	0.9606	0.7006	0.9857	4	40	0	82	all pixels
Lupaşcu et al. (2010)	0.9597	0.6728	0.9874	4	7	0	57	all pixels
Ricci and Perfetti (2007)	0.9595	0.7283	0.9832	4	2	0	50	outlier
Fathi and Naghsh-Nilchi (2013)	0.9581	0.7768	0.9759	4	20	0	100	all pixels
Dash and Bhoi (2018)	0.9570	0.7410	0.9860	3	20	15	10	outlier
Frucci et al. (2016)	0.9550	0.6400	0.9850	3	20	0	100	all pixels
Saroj et al. (2020)	0.9544	0.7307	0.9761	4	20	0	100	all pixels
GeethaRamani and Bal/an (2016)	0.9536	0.7079	0.9778	4	20	0	85	all pixels
Meng et al. (2015)	0.9529	0.7489	0.9818	4	20	5	0	outlier
Li et al. (2016)	0.9527	0.7569	0.9816	4	2	100	0	FoV
Imani et al. (2015)	0.9523	0.7524	0.9753	4	20	0	0	outlier
Singh and Srivastava (2016)	0.9522	0.7594	0.9708	4	20	0	100	all pixels
Mo and Zhang (2017)	0.9521	0.7760	0.9779	4	2	100	0	FoV
Dash et al. (2020)	0.9520	0.7560	0.9810	3	20	25	15	outlier
Singh and Srivastava (2017)	0.9513	0.7171	0.9739	4	20	0	100	all pixels
Bharkad (2017)	0.9503	0.7278	0.9718	4	20	0	100	all pixels
Barkana et al. (2017)	0.9502	0.7224	0.9840	4	4	0	0	outlier
Khan et al. (2016)	0.9501	0.7373	0.9670	4	20	0	5	outlier
Fraz et al. (2012c)	0.9480	0.7406	0.9807	4	2	0	0	outlier
Rahebi and Hardala (2014)	0.9461	0.7365	0.9707	4	20	5	0	outlier
Marin et al. (2011)	0.9452	0.7067	0.9801	4	20	100	0	FoV
Adapa et al. (2020)	0.9450	0.6994	0.9811	4	20	100	0	FoV
Kumar et al. (2020)	0.9432	0.7503	0.9717	4	20	100	0	FoV
Fraz et al. (2012a)	0.9430	0.7152	0.9769	4	2	50	0	outlier
Emary et al. (2014)	0.9390	0.7210	0.9710	3	20	100	0	FoV
Odstrcilik et al. (2013)	0.9340	0.7060	0.9693	4	20	0	0	outlier

3.4.1. The consistency test for aggregated figures

The concept of the consistency test for the average scores is similar to that of the image level test. Given the exact number of positive (vessel) and negative (non-vessel) pixels for each image in the DRIVE test set, one can formulate conditions that must be satisfied if the evaluation was performed according to the assumptions about the region of evaluation. Let $p_i^*, n_i^*, i = 1, \ldots, 20$ denote the number of positive and negative pixels in the manual annotation of the ith image under a particular assumption (the use of the FoV or all pixels). If the assumption is true, the following conditions must be satisfiable for some tp_i, tn_i, $i = 1, \ldots, 20$ unknown integers:

$$\overline{sens} - \epsilon \leq \frac{1}{20} \sum_{i=1}^{20} \frac{tp_i}{p_i^*} \leq \overline{sens} + \epsilon, \tag{6}$$

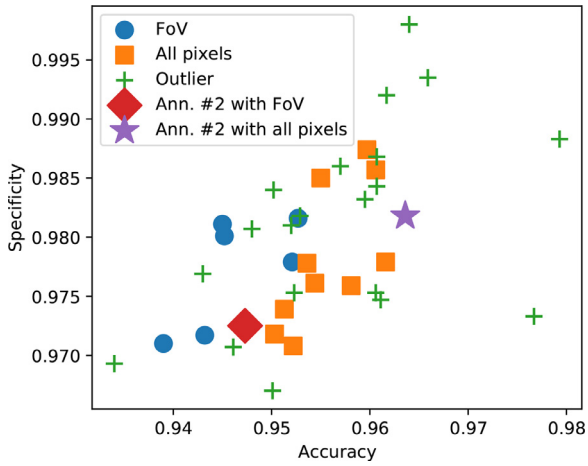

Fig. 3. The distribution of aggregated scores by the categories implied by image level figures.

$$\overline{spec} - \epsilon \leq \frac{1}{20}\sum_{i=1}^{20}\frac{tn_i}{n_i^*} \leq \overline{spec} + \epsilon, \tag{7}$$

$$\overline{acc} - \epsilon \leq \frac{1}{20}\sum_{i=1}^{20}\frac{tp_i + tn_i}{p_i^* + n_i^*} \leq \overline{acc} + \epsilon, \tag{8}$$

$$0 \leq tp_i \leq p_i^*, \quad 0 \leq tn_i \leq n_i^*, \quad i = 1, \ldots, 20. \tag{9}$$

All these conditions are linear functions of the unknowns, thus, (6)-(9) can be interpreted as the condition set of a linear integer programming problem. In order to check if these conditions can be fulfilled, one can exploit any linear integer programming solver with a dummy objective function, and an empty feasibility set returned by the solver indicates that the conditions cannot be satisfied, thus, the aggregated performance scores are not consistent with the test images of DRIVE under the hypothesis (using the FoV or all pixels) which led to the p_i^* and n_i^* numbers.

3.4.2. Sensitivity of the consistency test for aggregated figures

Similarly to the image level analysis, the aggregated figures must pass the test if the assumptions are met. However, due to the increased numerical uncertainty, it is questionable whether the sensitivity of the test is high enough to distinguish the two corner cases we are concerned with. As before, a quantitative characterization of sensitivity can be obtained by varying the size of the evaluation region, but this time checking whether the aggregated figures pass the test with the p_i^*, n_i^*, $i = 1, \ldots, 20$ numbers extracted according to the hypotheses. According to the results shown in Fig. 4, a 15% deviation in size from the hypothesised region causes the test to fail when the scores are reported to 4 digits. With rounding to 3 digits, the two corner cases are still distinguished by the test. However, if the region of evaluation is between 77%-87% of the image size, the scores can pass the test with either assumption.

3.4.3. The results on aggregated figures

In some papers (such as (Wu et al., 2020)), multiple triplets of aggregated scores are reported to illustrate the effects of the various steps of the proposed methods. Similarly to the image level analysis, the majority rule is applied to make clear decisions about the region of evaluation used by the authors. The results are summarized in Table 3 and plotted in Fig. 5. Again, we assigned 3 labels to the papers, in 30 cases the use of the FoV was accepted, in 18 cases the use of all pixels was accepted, and 16 papers were classified as outliers (the scores do not pass the test with either of the hypothesised regions). As before, the ranking in Table 3 and the illustration in Fig. 5 confirm the expected bias in the evaluations: the algorithms evaluated on all pixels tend to have higher accuracy and specificity scores, in general.

To assess the sensitivity of the aggregated consistency test compared to the image level test, we compared the categorization based on image level and aggregated figures and found that the aggregated consistency test gave the same result in all cases where the use of the FoV mask or all pixels was confirmed at the image level. However, from the total of 20 outliers identified at the image level, in 15 cases the aggregated scores passed the consistency test with one of the assumptions. This suggests that there can be further outliers among the papers in which only aggregated scores are reported and the consistency test confirmed one of the hypotheses.

3.5. An improved ranking

In this section, we attempt to derive a more realistic ranking of the algorithms by eliminating the bias caused by the differing regions of evaluation. The goal of the method we develop is to map the scores calculated on all pixels into the domain of evaluation with the FoV mask.

The idea is analogous to that of the consistency tests. Let the subscripts x_F and x_a refer to figures computed under the FoV mask and using all pixels, respectively, and let $x_d = x_a - x_F$ denote the difference. Given a particular triplet of image level scores acc_a, $sens_a$ and $spec_a$ reported by the authors with $\epsilon = 10^{-k}$ numerical uncertainty, we would like to infer on acc_F, $sens_F$ and $spec_F$. Substituting the unknowns $tp_a^* = tp_F^* + tp_d^*$ and $tn_a^* = tn_F^* + tn_d^*$ into (1)-(4), one gets the conditions

$$\begin{aligned}
sens_a - \epsilon &\leq \frac{tp_F^* + tp_d^*}{p_F^* + p_d^*} \leq sens_a + \epsilon \\
spec_a - \epsilon &\leq \frac{tn_F^* + tn_d^*}{n_F^* + n_d^*} \leq spec_a + \epsilon, \\
acc_a - \epsilon &\leq \frac{tp_F^* + tn_F^* + tp_d^* + tn_d^*}{p_F^* + n_F^* + p_d^* + n_d^*} \leq acc_a + \epsilon, \\
tp_F^* &\in [0, p_F^*], \quad tn_F^* \in [0, n_F^*], \quad tp_d^* \in \left[0, p_d^*\right], \quad tn_d^* \in \left[0, n_d^*\right],
\end{aligned} \tag{10}$$

which must hold for some integer unknowns tp_F^*, tn_F^*, tp_d^* and tn_d^*. The constants p_F^*, p_d^*, n_F^* and n_d^* are known from the publicly available test set. Focusing on the accuracy score $acc_F^* = \frac{tp_F^* + tn_F^*}{p_F^* + n_F^*}$ first, we are interested in a lower and upper bound on the values it can take under the conditions (10). Recognizing that the conditions (10) with the objective function acc_F^* form a linear integer programming problem of the free integer variables tp_F^*, tn_F^*, tp_d^* and tn_d^*, one can determine the minimum (L) and maximum (U) values the objective function can take by exploiting any linear programming solver. These extrema provide a sharp interval estimate for the accuracy score evaluated under the FoV: $acc_F^* \in [L(acc_F^*), U(acc_F^*)]$. The adjusted accuracy score is defined as the mid-point of the interval and the error of the adjustment is estimated as the half-width of the interval:

$$acc_F' = \frac{L(acc_F^*) + U(acc_F^*)}{2}, \quad \epsilon\left(acc_F'\right) = \frac{U(acc_F^*) - L(acc_F^*)}{2}. \tag{11}$$

The adjusted image level $sens_F'$ and $spec_F'$ scores and corresponding error estimates are determined analogously.

In practice, we found that the formulation (10) leads to wide intervals due to mathematical solutions that are not aligned with the problem. In the formulation (10), the number of true negatives outside the FoV (tn_d) can be zero, that is, the linear programming solver considers variable configurations corresponding to segmentations where all pixels outside the FoV are segmented as vessels,

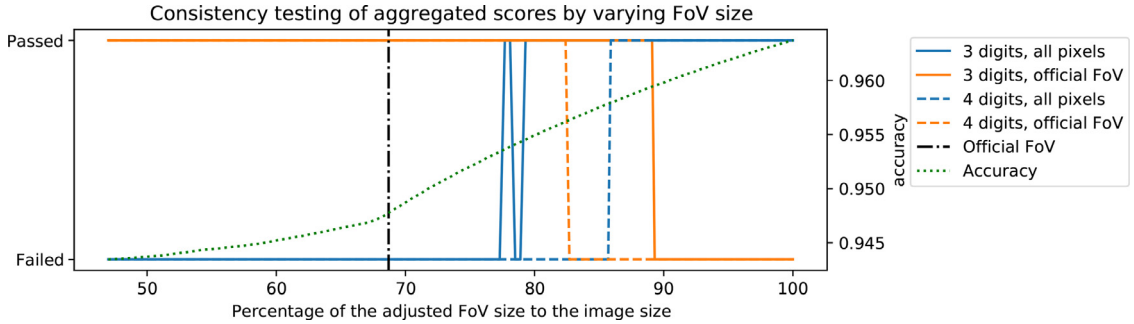

Fig. 4. Indicator curves for the aggregated scores showing whether the scores pass the consistency tests with the two assumptions when the region of evaluation and the rounding of performance scores are varied.

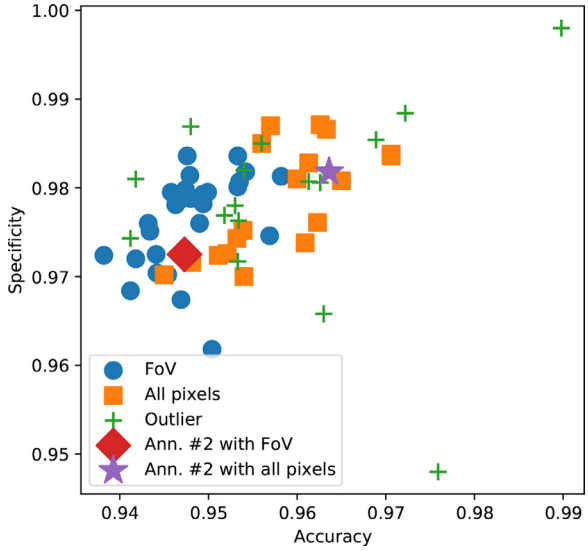

Fig. 5. The distribution of aggregated scores by the categories implied by the aggregated figures.

which is unlikely. In order to tighten the intervals, the configuration space is reduced by making the natural assumption that no more negative pixels than 1% of the vasculature are segmented as vessels outside the FoV: $tn_d \in \left[n^*_d - 0.01p^*_F, n^*_d\right]$. With this constraint, the worst-case error of the adjustment when applied to all image level figures reduces to 0.002 with the average of 0.001, which we found sufficiently tight for further analysis.

Similarly to the image level adjustment, for the averaged scores, one can substitute $tp^*_{a,i} = tp^*_{F,i} + tp^*_{d,i}$ and $tn^*_{a,i} = tn^*_{F,i} + tn^*_{d,i}$, $i = 1, \ldots, 20$ into the conditions (6) - (9) leading to a set of linear integer constraints. Then, minimizing and maximizing the objective function

$$\overline{acc}^*_F = \sum_{i=1}^{20} \frac{tp^*_{F,i} + tn^*_{F,i}}{p^*_{F,i} + n^*_{F,i}} \tag{12}$$

in the free integer variables $tp^*_{F,i}, tn^*_{F,i}, tp^*_{d,i}, tn^*_{d,i}$, $i = 1, \ldots, 20$, one gets a sharp interval estimate for $\overline{acc}^*_F$. The adjusted aggregated score $\overline{acc}_F{}'$ is determined as the mid-point of the interval and the corresponding error term $\epsilon_{\overline{acc}_F}$ as the half-width of the interval. The adjusted $\overline{sens}^*_F$ and $\overline{spec}^*_F$ scores are determined analogously.

For illustration, the adjustment was applied to the scores calculated on all pixels and reported in our earlier paper (Kovács and Hajdu, 2016). The adjusted scores $\overline{acc}'_F = 0.9500$, $\overline{sens}'_F = 0.7447$, $\overline{spec}'_F = 0.9802$ are well aligned with the true scores $\overline{acc}_F = 0.9494$, $\overline{sens}_F = 0.7446$, $\overline{spec}_F = 0.9793$ calculated in the FoV area, the error of the adjustment is not higher than 0.001 for any of the figures.

The adjustment was applied to the reported scores of all methods we identified to be evaluated using all pixels. The worst case of the adjustment is 0.003 with the average of 0.001. As the errors are an order of magnitude smaller than the bias, we believe that the ranking based on the adjusted scores in Table 4 is a more reliable baseline for the field than the original ranking in Table 1.

4. Insights

Based on the raw results and the adjusted scores, in this section, we provide some detailful insights into the field.

4.1. Insights from the consistency testing

Overall, the use of the FoV mask was accepted in 36 cases, and the scores reported in 28 papers were consistent with the use of all pixels for evaluation. 36 papers were found to be outliers with undoubtful evidence that the evaluation was carried out in an unknown third way. Binomial hypothesis testing at the usual significance levels fails to reject the null hypothesis that the authors have no preference in the choice of the evaluation methodology (p-value: 0.19). Consequently, we can state that *neither of the two evaluation methodologies we investigated can be treated as a standard in the field.*

Explicit phrasing of the region of evaluation was found only in 29 papers. Out of them, only in 15 cases were the reported scores consistent with the claims of the authors. These inconsistencies indicate that *the most reliable source for the region of evaluation is the triplet of performance scores the authors shared.*

The results of the consistency tests can be used to verify that the rankings in the papers are valid: if at least two algorithms evaluated in different regions are included in a ranking, it contains non-comparable figures. This phenomenon was confirmed in 91 of the 100 papers. Together with the 10 reviews (Almotiri et al., 2018; Moccia et al., 2018; Mookiah et al., 2021; Besenczi et al., 2016; Khan et al., 2018; Cetinkaya and Duran, 2020; Srinidhi et al., 2017; Singh et al., 2020; Fraz et al., 2012b; Fu et al., 2018) which only recite published figures, the statement in the title of this paper is confirmed: *rankings are based on non-comparable figures in 100+ papers.* As recent papers are also affected, we can conclude that *ranking algorithms based on non-comparable figures is an existing and ongoing problem in the field.*

4.2. Insights from the new ranking

The correlation coefficient between the original and the adjusted rankings is 0.18, indicating that *the adjustment of scores leads to a substantial change in the recognition of efficient vessel segmentation techniques.*

The reported scores show that the accuracy of annotator #2 was outperformed by 1% in 2007, and at the time of writing,

Table 3
The results of the consistency tests for aggregated figures, '+' denoting the cases passing the test with a particular assumption.

Key	$\overline{acc}$	$\overline{sens}$	$\overline{spec}$	Decimal places	Num. agg. figures	Passed assum. FoV	Passed assum. all pixels	Decision
Jebaseeli et al. (2019)	0.9898	0.8027	0.9980	4	1			outlier
Villalobos-Castaldi et al. (2010)	0.9759	0.9649	0.9480	4	1			outlier
Memari et al. (2017)	0.9722	0.8726	0.9884	4	1			outlier
Park et al. (2020)	0.9706	0.8346	0.9836	4	1		+	all pixels
Jiang et al. (2019)	0.9706	0.8325	0.9838	4	1		+	all pixels
Atli and Gedik (2021)	0.9689	0.7987	0.9854	4	1			outlier
Xiuqin et al. (2019)	0.9650	0.8150	0.9808	4	1		+	all pixels
Sreejini and Govindan (2015)	0.9633	0.7132	0.9866	4	1		+	all pixels
Saleh et al. (2011)	0.9630	0.8423	0.9658	4	1			outlier
Kumar et al. (2016)	0.9626	0.7006	0.9871	4	1		+	all pixels
Wankhede and Khanchandani (2015)	0.9626	0.7261	0.9806	4	1			outlier
Pandey et al. (2017)	0.9623	0.8106	0.9761	4	1		+	all pixels
Alom et al. (2019)	0.9613	0.7661	0.9807	4	1			outlier
Xiang et al. (2014)	0.9613	0.7538	0.9828	4	1		+	all pixels
Samuel and Veeramalai (2019)	0.9609	0.8282	0.9738	4	1		+	all pixels
Fan et al. (2017)	0.9600	0.7360	0.9810	3	1		+	all pixels
Wu et al. (2020)	0.9582	0.7996	0.9813	4	1	+		FoV
Budai et al. (2013)	0.9570	0.6440	0.9870	3	1		+	all pixels
Noh et al. (2019)	0.9569	0.8354	0.9746	4	1	+		FoV
Soomro et al. (2019)	0.9560	0.8700	0.9850	3	1			outlier
Frucci et al. (2017)	0.9560	0.6600	0.9850	3	1		+	all pixels
Yan et al. (2018)	0.9542	0.7653	0.9818	4	1	+		FoV
Na et al. (2018)	0.9540	0.7680	0.9700	3	1		+	all pixels
Zhao et al. (2015b)	0.9540	0.7420	0.9820	3	1			outlier
Panda et al. (2016)	0.9539	0.7328	0.9752	4	1		+	all pixels
Liskowski and Krawiec (2016)	0.9535	0.7811	0.9807	4	1	+		FoV
Soomro et al. (2018)	0.9534	0.7592	0.9763	4	1			outlier
Dasgupta and Singh (2017)	0.9533	0.7691	0.9801	4	1	+		FoV
Hu et al. (2018)	0.9533	0.7796	0.9717	4	1			outlier
Ngo and Han (2017)	0.9533	0.7464	0.9836	4	1	+		FoV
Yang et al. (2020)	0.9532	0.7349	0.9743	4	1		+	all pixels
Zhao et al. (2015a)	0.9530	0.7440	0.9780	3	1			outlier
Isavand Rahmani et al. (2020)	0.9521	0.7400	0.9726	4	1		+	all pixels
Chalakkal and Abdulla (2017)	0.9518	0.7386	0.9769	4	1			outlier
Mapayi et al. (2015)	0.9511	0.7313	0.9724	4	1		+	all pixels
Zhang and Chung (2018)	0.9504	0.8723	0.9618	4	1	+		FoV
Song and Lee (2017)	0.9499	0.7501	0.9795	4	1	+		FoV
Roychowdhury et al. (2015)	0.9494	0.7395	0.9782	4	1	+		FoV
Kovács and Hajdu (2016)	0.9494	0.7450	0.9793	4	1	+		FoV
Brancati et al. (2018)	0.9490	0.7820	0.9760	3	1	+		FoV
Nazari and Pourghassem (2013)	0.9481	0.7112	0.9716	4	1		+	all pixels
Kaur and Mittal (2017)	0.9480	0.8730	0.9869	4	1			outlier
Palanivel et al. (2020)	0.9480	0.7375	0.9788	4	1	+		FoV
Shah et al. (2017)	0.9479	0.7205	0.9814	4	1	+		FoV
Zhang et al. (2016)	0.9476	0.7743	0.9725	4	1	+		FoV
Shukla et al. (2020)	0.9476	0.7015	0.9836	4	1	+		FoV
Cheng et al. (2014)	0.9474	0.7252	0.9798	4	1	+		FoV
Zhou et al. (2017)	0.9469	0.8078	0.9674	4	1	+		FoV
Melinscak et al. (2015)	0.9466	0.7276	0.9785	4	1	+		FoV
Rezaee et al. (2017)	0.9463	0.7189	0.9793	4	1	+		FoV
Mendonca and Campilho (2006)	0.9463	0.7315	0.9781	4	1	+		FoV
Miri and Mahloojifar (2010)	0.9458	0.7352	0.9795	4	1	+		FoV
Strisciuglio et al. (2016)	0.9454	0.7777	0.9702	4	1	+		FoV
Javidi et al. (2017)	0.9450	0.7201	0.9702	4	1		+	all pixels
Strisciuglio et al. (2015)	0.9442	0.7655	0.9704	4	1	+		FoV
Azzopardi et al. (2015)	0.9442	0.7655	0.9704	4	1	+		FoV
Staal et al. (2004)	0.9441	0.7750	0.9725	4	1	+		FoV
You et al. (2011)	0.9434	0.7410	0.9751	4	1	+		FoV
Soomro et al. (2017)	0.9432	0.7523	0.9760	4	1	+		FoV
Dai et al. (2015)	0.9418	0.7359	0.9720	4	1	+		FoV
Anzalone et al. (2008)	0.9418	0.7286	0.9810	4	1			outlier
Dizdaroglu et al. (2012)	0.9412	0.7181	0.9743	4	1			outlier
Salazar et al. (2014)	0.9412	0.7512	0.9684	4	1	+		FoV
Zhang et al. (2010)	0.9382	0.7120	0.9724	4	1	+		FoV

near-perfect techniques are available with accuracy of 0.98-0.99. In contrast, the adjusted scores show that the accuracy of annotator #2 was only reached in 2014, and the highest accuracy to date is only 1% above it (evaluated under the FoV mask). This phenomenon shows similarities with the field of electrohysterogram classification: the near perfect accuracy scores reported in the literature were caused by a methodological flaw in the evaluations (Vandewiele et al., 2021).

In Fig. 6a we have plotted the distribution of algorithms and evaluation methodologies in the adjusted accuracy-specificity plane. The plot shows that after eliminating the bias, *the algorithms evaluated with all pixels have lower accuracy and specificity*

Table 4
The improved ranking based on adjusted performance scores, without outliers.

Key	Rank	Original rank	Rank diff.	Adjusted acc.	Published acc.	Category	Operation
Wu et al. (2020)	1	30	29	0.9582	0.9582	FoV	deep learning
Park et al. (2020)	2	6	4	0.9578	0.9706	all pixels	deep learning
Jiang et al. (2019)	3	7	4	0.9578	0.9706	all pixels	deep learning
Noh et al. (2019)	4	34	30	0.9569	0.9569	FoV	deep learning
Yan et al. (2018)	5	39	34	0.9542	0.9542	FoV	deep learning
Liskowski and Krawiec (2016)	6	44	38	0.9535	0.9535	FoV	deep learning
Ngo and Han (2017)	7	47	40	0.9533	0.9533	FoV	deep learning
Dasgupta and Singh (2017)	8	46	38	0.9533	0.9533	FoV	deep learning
Li et al. (2016)	9	52	43	0.9527	0.9527	FoV	deep learning
Mo and Zhang (2017)	10	55	45	0.9521	0.9521	FoV	deep learning
Xiuqin et al. (2019)	11	10	-1	0.9505	0.9650	all pixels	deep learning
Zhang and Chung (2018)	12	61	49	0.9504	0.9504	FoV	deep learning
Song and Lee (2017)	13	65	52	0.9499	0.9499	FoV	deep learning
Roychowdhury et al. (2015)	14	67	53	0.9494	0.9494	FoV	classical
Kovács and Hajdu (2016)	15	66	51	0.9494	0.9494	FoV	classical
Brancati et al. (2018)	16	68	52	0.9490	0.9490	FoV	deep learning
Palanivel et al. (2020)	17	71	54	0.9480	0.9480	FoV	supervised
Shah et al. (2017)	18	73	55	0.9479	0.9479	FoV	supervised
Zhang et al. (2016)	19	74	55	0.9476	0.9476	FoV	classical
Shukla et al. (2020)	20	75	55	0.9476	0.9476	FoV	classical
Cheng et al. (2014)	21	76	55	0.9474	0.9474	FoV	supervised
Sreejini and Govindan (2015)	22	12	-10	0.9471	0.9633	all pixels	classical
Zhou et al. (2017)	23	77	54	0.9469	0.9469	FoV	other
Melinscak et al. (2015)	24	78	54	0.9466	0.9466	FoV	deep learning
Rezaee et al. (2017)	25	80	55	0.9463	0.9463	FoV	classical
Mendonca and Campilho (2006)	26	79	53	0.9463	0.9463	FoV	classical
Kumar et al. (2016)	27	14	-13	0.9463	0.9626	all pixels	classical
Miri and Mahloojifar (2010)	28	82	54	0.9458	0.9458	FoV	classical
Pandey et al. (2017)	29	16	-13	0.9458	0.9623	all pixels	classical
Strisciuglio et al. (2016)	30	83	53	0.9454	0.9454	FoV	supervised
Xiang et al. (2014)	31	19	-12	0.9452	0.9613	all pixels	classical
Marin et al. (2011)	32	84	52	0.9452	0.9452	FoV	supervised
Adapa et al. (2020)	33	85	52	0.9450	0.9450	FoV	supervised
Waheed et al. (2015)	34	18	-16	0.9447	0.9616	all pixels	supervised
Azzopardi et al. (2015)	35	87	52	0.9442	0.9442	FoV	classical
Strisciuglio et al. (2015)	36	88	52	0.9442	0.9442	FoV	classical
Staal et al. (2004)	37	89	52	0.9441	0.9441	FoV	supervised
Samuel and Veeramalai (2019)	38	22	-16	0.9437	0.9609	all pixels	deep learning
You et al. (2011)	39	90	51	0.9434	0.9434	FoV	supervised
Lupascu and Tegolo (2016)	40	26	-14	0.9433	0.9606	all pixels	other
Soomro et al. (2017)	41	91	50	0.9432	0.9432	FoV	classical
Kumar et al. (2020)	42	92	50	0.9432	0.9432	FoV	classical
Fan et al. (2017)	43	27	-16	0.9421	0.9600	all pixels	classical
Lupaşcu et al. (2010)	44	28	-16	0.9421	0.9597	all pixels	supervised
Dai et al. (2015)	45	94	49	0.9418	0.9418	FoV	classical
Salazar et al. (2014)	46	97	51	0.9412	0.9412	FoV	other
Fathi and Naghsh-Nilchi (2013)	47	31	-16	0.9397	0.9581	all pixels	classical
Emary et al. (2014)	48	98	50	0.9390	0.9390	FoV	classical
Zhang et al. (2010)	49	99	50	0.9382	0.9382	FoV	classical
Budai et al. (2013)	50	33	-17	0.9381	0.9570	all pixels	classical
Frucci et al. (2017)	51	36	-15	0.9366	0.9560	all pixels	classical
Frucci et al. (2016)	52	37	-15	0.9348	0.9550	all pixels	classical
Saroj et al. (2020)	53	38	-15	0.9344	0.9544	all pixels	classical
Panda et al. (2016)	54	42	-12	0.9336	0.9539	all pixels	classical
GeethaRamani and Bal/an (2016)	55	43	-12	0.9330	0.9536	all pixels	supervised
Yang et al. (2020)	56	49	-7	0.9325	0.9532	all pixels	classical
Na et al. (2018)	57	41	-16	0.9325	0.9540	all pixels	classical
Singh and Srivastava (2016)	58	54	-4	0.9311	0.9522	all pixels	classical
Isavand Rahmani et al. (2020)	59	56	-3	0.9309	0.9521	all pixels	classical
Singh and Srivastava (2017)	60	59	-1	0.9298	0.9513	all pixels	classical
Mapayi et al. (2015)	61	60	-1	0.9295	0.9511	all pixels	classical
Bharkad (2017)	62	62	0	0.9284	0.9503	all pixels	classical
Nazari and Pourghassem (2013)	63	69	6	0.9250	0.9481	all pixels	classical
Javidi et al. (2017)	64	86	22	0.9231	0.9450	all pixels	supervised

scores than those evaluated with the FoV mask. The independent two-sample *t*-test shows that the difference is statistically significant with a p-value of 10^{-9}. The reason for this surprising phenomenon is that using all pixels to evaluate less effective techniques results in performance scores comparable to or even higher than those of more effective techniques evaluated under the FoV mask, and this brings publicity to less effective approaches.

Finally, we compare the performances of the methods by their operating principles. We have introduced 4 categories: deep learning, classical (thresholding, filtering, morphology, region growing), supervised (feature extraction and supervised machine learning, but not deep learning), and others (dominantly graph-cut based segmentation techniques). The results presented in Fig. 6b show that *deep learning techniques increase the accuracy by al-*

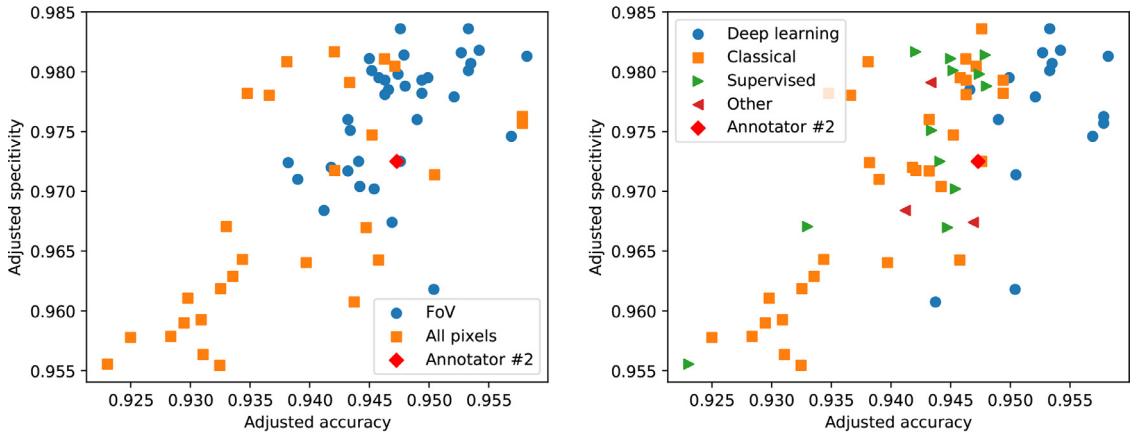

(a) (b)

Fig. 6. The distribution of the adjusted figures in the accuracy-specificity plane: by evaluation methodologies (a); and operating principles (b).

most 1% compared to the best performing classical and supervised techniques.

4.3. A remark on the evaluation of deep learning techniques

From a development perspective, there is an important difference between heuristic image processing pipelines and highly flexible deep learning solutions that calls into question the suitability of current evaluation methodologies in the field. Unlike the heuristic improvement of conventional image processing pipelines, the tuning of hyperparameters in deep neural networks is relatively straightforward (automated in many cases), which increases the risk of overfitting when the performance scores measured on the test set drive the tuning of the network.

Although this could be prevented by using the training images of DRIVE for both training the weights in the network and tuning the network structure, we found evidence that some results are clearly overfitted to the test set: Both (Li et al., 2016) and (Liskowski and Krawiec, 2016) optimize the network size and hyperparameters on the test images. Despite the obvious overfitting, we did not discard these results for two reasons. First, all other papers using deep learning declare the network structures and the hyperparameters. None of the authors describe how the network was derived from the training data, which risks the overfitting of the network structure to the test images. On the other hand, there is no doubt that deep learning techniques achieve better results than classical approaches. Although some papers may have reported too optimistic scores due to overfitting to the test images, they clearly dominate the field.

Consequently, the development and evaluation of deep learning solutions for retinal vessel segmentation should follow the standards of the deep learning literature by using 3 sets of images (Larochelle et al., 2009): one to train the weights in the network, another to tune the network structure and a final one to test the performance of the optimised network. However, since DRIVE specifies only 2 subsets and further splitting of the training set (20 images) would lead to a nearly insufficient number of images for deep learning, a larger set of images should become the standard in this field.

4.4. Limitations

The analysis we carried out has numerous limitations. Despite the systematic search for influential papers, the selected group may provide a biassed representation of the field and the results of the selection process may change over time as the number of citations changes.

The consistency tests for aggregated figures tolerate greater deviation from the hypotheses than do the image level tests. This inherent imbalance in the rigour of the tests implies that some papers that passed the consistency test with aggregated scores might have failed if the authors had reported image level scores.

The adjusted scores have some numerical uncertainty. Although the estimated errors are small, the improved ranking is also uncertain to this degree.

We have focused primarily on the comparability of the reported performance scores. However, higher performance is not the only goal in science. If some methods are easier to understand, maintain, adapt, or are more efficient in terms of runtime, they are still valuable contributions to science. Therefore, the improved ranking does not devalue the contributions of any paper, as all papers provide insights into the capabilities of the implemented approaches.

5. Summary and conclusions

In this study, we investigated the coherence of reported performance scores in the segmentation of vessels in retinal images. We collected 100 influential papers reporting accuracy, sensitivity, and specificity for the publicly available data set DRIVE. Based on textual references to two corner cases of evaluation methodologies (evaluation under the FoV mask or using all pixels of the images), we developed numerical methods to test the consistency of the reported scores with the two assumed corner cases (Subsections 3.3.1, 3.4.1). Based on results of consistency tests, we attempted to remove bias and make the scores comparable to create a new baseline ranking (Section 3.5). Section 4 summarizes various findings and insights and also discusses the limitations of our analysis. The insights clearly show that there is no consensus in the field on the evaluation methodology. However, in most of the papers, including reviews of the field, the rankings and the objective evaluation of operating principles are biassed by the direct comparison of non-comparable figures. Based on the papers we selected and the adjustment we implemented, the current state of the art accuracy is 0.9582 (evaluated in the FoV region), which is about 1.1% higher than the performance of annotator #2. Despite the limitations of our method, we believe that the adjusted ranking in Table 4 provides a more realistic view of the state of the art than any ranking based on the direct comparison of reported figures.

The findings have numerous implications regarding the suitability and potential improvements of data sets, evaluation methodologies and reporting standards in the field:

- *A novel data set that takes into account the changing requirements of the field is desirable* - potentially, this could emerge as a curated fusion of existing vessel segmentation data sets that provides predefined training, test and validation subsets for the reliable evaluation of deep learning techniques, and the sizes of the subsets should be based on well-established principles (Guyon et al., 1998).
- The published average scores on DRIVE usually differ in the 3th-4th digits. Since these are the averages of only 20 image level scores, one can assume a relatively large variance, which makes the rankings ambigious. To investigate whether there were statistically significant improvements, *the authors should provide image level figures* at least as supplementary material and explicitly report more details about the evaluation methodology (e.g., the region they use to calculate the scores).
- *Authors should report the* Dice score (Eelbode et al., 2020), $dice = (2 \cdot tp)/(2 \cdot tp + fp + fn)$, which is a commonly accepted measure of segmentation performance. Since *dice* is inherently free of the number of true negatives, the bias we study in this paper is naturally eliminated. Treating retinal vessel segmentation as a pixelwise binary classification problem, the AUC score (the standard performance measure for binary classification in machine learning) provides good insight into the trade-off between the sensitivity and specificity of segmentation algorithms - *if applicable (the segmentation is based on pixelwise vesselness probabilities), authors should report AUC scores.*
- Maximizing some pixelwise performance measures of segmentation does not necessarily improve clinical applications. For example, an algorithm that provides an average accuracy of 0.95 with a small standard deviation may lead to a more reliable grading of disease severity than an algorithm with an average accuracy of 0.96 and a huge standard deviation, which means that it fails under certain conditions. Consequently, *the evaluation of vessel segmentation methods should be more closely linked to clinical applications.*

The numerical techniques we have developed can be easily adapted to other problems where similar methodological flaws may arise. To allow full reproducibility and further analysis, all raw data, the implementation of the analysis and all results are shared in the GitHub repository www.github.com/gykovacs/retinal_vessel_segmentation.

Declaration of Competing Interest

The authors declare that they have no known competing financial interests or personal relationships that could have appeared to influence the work reported in this paper.

CRediT authorship contribution statement

György Kovács: Conceptualization, Methodology, Software, Writing – original draft. **Attila Fazekas:** Data curation, Writing – original draft, Validation, Writing – review & editing.

Acknowledgments

György Kovács would like to thank the support of the initiative 1LU-51P-4E. On behalf of Attila Fazekas, this work was supported by the construction EFOP-3.6.3-VEKOP-16-2017-00002. The project was supported by the European Union, co-financed by the European Social Fund.

References

Abramoff, M., Garvin, M., Sonka, M., 2010. Retinal imaging and image analysis. Biomedical Engineering, IEEE Reviews in 3, 169–208. doi:10.1109/RBME.2010.2084567.

Adapa, D., Joseph Raj, A.N., Alisetti, S.N., Zhuang, Z., K, G., Naik, G., 2020. A supervised blood vessel segmentation technique for digital fundus images using zernike moment based features. PLoS ONE 15 (3), 1–23. doi:10.1371/journal.pone.0229831.

Almotiri, J., Elleithy, K., Elleithy, A., 2018. Retinal vessels segmentation techniques and algorithms: a survey. Applied Sciences 8. doi:10.3390/app8020155.

Alom, M.Z., Yakopcic, C., Hasan, M., Taha, T., Asari, V., 2019. Recurrent residual u-net for medical image segmentation. J. Med. Imaging 6. doi:10.1117/1.JMI.6.1.014006.

Anzalone, A., Bizzarri, F., Parodi, M., Storace, M., 2008. A modular supervised algorithm for vessel segmentation in red-free retinal images. Comput. Biol. Med 38 (8), 913—922. doi:10.1016/j.compbiomed.2008.05.006.

Atli, I., Gedik, O.S., 2021. Sine-net: a fully convolutional deep learning architecture for retinal blood vessel segmentation. Engineering Science and Technology, an International Journal 24 (2), 271–283. doi:10.1016/j.jestch.2020.07.008.

Azzopardi, G., Strisciuglio, N., Vento, M., Petkov, N., 2015. Trainable cosfire filters for vessel delineation with application to retinal images. Med Image Anal 19 (1), 46–57. doi:10.1016/j.media.2014.08.002.

Barkana, B., Saricicek, I., Yildirim, B., 2017. Performance analysis of descriptive statistical features in retinal vessel segmentation via fuzzy logic, ann, svm, and classifier fusion. Knowl Based Syst 118. doi:10.1016/j.knosys.2016.11.022.

Besenczi, R., Tóth, J., Hajdu, A., 2016. A review on automatic analysis techniques for color fundus photographs. Comput Struct Biotechnol J 14, 371–384. doi:10.1016/j.csbj.2016.10.001.

Bharkad, S., 2017. Automatic segmentation of blood vessels in retinal image using morphological filters. In: Proceedings of the 6th International Conference on Software and Computer Applications - ICSCA17. ACM Press doi:10.1145/3056662.3056710.

Brancati, N., Frucci, M., Gragnaniello, D., Riccio, D., 2018. Retinal Vessels Segmentation Based on a Convolutional Neural Network, pp. 119–126.

Budai, A., Bock, R., Maier, A., Hornegger, J., Michelson, G., 2013. Robust vessel segmentation in fundus images. Int J Biomed Imaging 2013.

Cetinkaya, M.B., Duran, H., 2020. A detailed and comparative work for retinal vessel segmentation based on the most effective heuristic approaches. Biomedical Engineering / Biomedizinische Technik 0 (0). doi:10.1515/bmt-2020-0089.

Chalakkal, R.J., Abdulla, W., 2017. Automatic segmentation of retinal vasculature. In: 2017 IEEE International Conference on Acoustics, Speech and Signal Processing (ICASSP), pp. 886–890. doi:10.1109/ICASSP.2017.7952283.

Cheng, E., Du, L., Wu, Y., Zhu, Y., Megalooikonomou, V., Ling, H., 2014. Discriminative vessel segmentation in retinal images by fusing context-aware hybrid features. Mach Vis Appl 25, 1779–1792. doi:10.1007/s00138-014-0638-x.

Computational retinal image analysis, 2019. In: Trucco, E., MacGillivray, T., Xu, Y. (Eds.). Elsevier doi:10.1016/c2018-0-00865-8.

Dai, P., Luo, H., Sheng, H., Zhao, Y., Li, L., Wu, J., Zhao, Y., Suzuki, K., 2015. A new approach to segment both main and peripheral retinal vessels based on gray-voting and gaussian mixture model. PLoS ONE 10 (6), 1–22. doi:10.1371/journal.pone.0127748.

Dasgupta, A., Singh, S., 2017. A fully convolutional neural network based structured prediction approach towards the retinal vessel segmentation. In: 2017 IEEE 14th International Symposium on Biomedical Imaging (ISBI 2017), pp. 248–251. doi:10.1109/ISBI.2017.7950512.

Dash, J., Bhoi, N., 2018. An unsupervised approach for extraction of blood vessels from fundus images. J Digit Imaging 31, 857–868.

Dash, J., Priyadarsan, P., Nilamani, B., 2020. Retinal blood vessel extraction from fundus images using enhancement filtering and clustering. ELCVIA: electronic letters on computer vision and image analysis 19 (1), 38–52.

Dizdaroglu, B., Cansizoglu, E., Kalpathy-Cramer, J., Keck, K., Chiang, M., ErdomuÅ, D., 2012. Level sets for retinal vasculature segmentation using seeds from ridges and edges from phase maps. 2012 IEEE International Workshop on Machine Learning for Signal Processing 1–6.

Eelbode, T., Bertels, J., Berman, M., Vandermeulen, D., Maes, F., Bisschops, R., Blaschko, M.B., 2020. Optimization for medical image segmentation: theory and practice when evaluating with dice score or jaccard index. IEEE Trans Med Imaging 39 (11), 3679–3690. doi:10.1109/TMI.2020.3002417.

Emary, E., Zawbaa, H., Hassanien, A.E., Schaefer, G., Azar, A., 2014. Retinal blood vessel segmentation using bee colony optimisation and pattern search doi:10.1109/IJCNN.2014.6889856.

Escorcia-Gutierrez, J., Torrents-Barrena, J., Gamarra, M., Romero-Aroca, P., Valls, A., Puig, D., 2020. Convexity shape constraints for retinal blood vessel segmentation and foveal avascular zone detection. Comput. Biol. Med. 127, 104049. doi:10.1016/j.compbiomed.2020.104049.

Fan, Z., Lu, J., Li, W., Wei, C., Huang, H., Cai, X., Chen, X., 2017. A hierarchical image matting model for blood vessel segmentation in fundus images. 1701.00892.

Fathi, A., Naghsh-Nilchi, A.R., 2013. Automatic wavelet-based retinal blood vessels segmentation and vessel diameter estimation. Biomed Signal Process Control 8 (1), 71–80. doi:10.1016/j.bspc.2012.05.005.

Fraz, M., Barman, S., Remagnino, P., Hoppe, A., Basit, A., Uyyanonvara, B., Rudnicka, A., Owen, C., 2012. An approach to localize the retinal blood vessels using bit planes and centerline detection. Comput Methods Programs Biomed 108 (2), 600–616. doi:10.1016/j.cmpb.2011.08.009.

Fraz, M., Remagnino, P., Hoppe, A., Uyyanonvara, B., Rudnicka, A., Owen, C., Barman, S., 2012. Blood vessel segmentation methodologies in retinal images - a survey. Comput Methods Programs Biomed 108, 407–433. doi:10.1016/j.cmpb.2012.03.009.

Fraz, M.M., Remagnino, P., Hoppe, A., Uyyanonvara, B., Rudnicka, A.R., Owen, C.G., Barman, S.A., 2012. An ensemble classification-based approach applied to retinal blood vessel segmentation. IEEE Trans Biomed Eng 59 (9), 2538–2548. doi:10.1109/tbme.2012.2205687.

Frucci, M., Riccio, D., Sanniti di Baja, G., Serino, L., 2017. Direction-based segmentation of retinal blood vessels. In: Beltrán-Castañón, C., Nyström, I., Famili, F. (Eds.), Progress in Pattern Recognition, Image Analysis, Computer Vision, and Applications. Springer International Publishing, Cham, pp. 1–9.

Frucci, M., Riccio, D., di Baja, G.S., Serino, L., 2016. Severe: segmenting vessels in retina images. Pattern Recognit Lett 82, 162–169. doi:10.1016/j.patrec.2015.07.002.

Fu, D., Liu, Y., Huang, Z., 2018. A review of retinal vessel segmentation and artery/vein classification. In: Jia, Y., Du, J., Zhang, W. (Eds.), Proceedings of 2017 Chinese Intelligent Systems Conference. Springer Singapore, Singapore, pp. 727–737.

GeethaRamani, R., Bal/an, L., 2016. Retinal blood vessel segmentation employing image processing and data mining techniques for computerized retinal image analysis. Biocybernetics and Biomedical Engineering 36 (1), 102–118. doi:10.1016/j.bbe.2015.06.004.

Guyon, I., Makhoul, J., Schwartz, R.M., Vapnik, V., 1998. What size test set gives good error rate estimates? IEEE Trans. Pattern Anal. Mach. Intell 20 (1), 52–64.

Hanley, J., Mcneil, B., 1982. The meaning and use of the area under a receiver operating characteristic (roc) curve. Radiology 143, 29–36. doi:10.1148/radiology.143.1.7063747.

Hassanien, A.E., 2018. Retinal fundus vasculature multilevel-segmentation using whale optimization algorithm. Signal Image Video Process 12. doi:10.1007/s11760-017-1154-z.

Hoover, A.D., Kouznetsova, V., Goldbaum, M., 2000. Locating blood vessels in retinal images by piecewise threshold probing of a matched filter response. IEEE Trans Med Imaging 19 (3), 203–210. doi:10.1109/42.845178.

Hu, K., Zhang, Z., Niu, X., Zhang, Y., Cao, C., Xiao, F., Gao, X., 2018. Retinal vessel segmentation of color fundus images using multiscale convolutional neural network with an improved cross-entropy loss function. Neurocomputing 309, 179–191. doi:10.1016/j.neucom.2018.05.011.

lui Cheung, C.Y., Ikram, M.K., Sabanayagam, C., Wong, T.Y., 2012. Retinal microvasculature as a model to study the manifestations of hypertension. Hypertension 60 (5), 1094–1103. doi:10.1161/hypertensionaha.111.189142.

Imani, E., Javidi, M., Pourreza, H.-R., 2015. Improvement of retinal blood vessel detection using morphological component analysis. Comput Methods Programs Biomed 118 (3), 263–279. doi:10.1016/j.cmpb.2015.01.004.

Isavand Rahmani, A., Akbari, H., Saraf Esmaili, S., 2020. Retinal blood vessel segmentation using gabor filter and morphological reconstruction. Signal Processing and Renewable Energy 4 (1), 77–88.

Javidi, M., Pourreza, H.-R., Harati, A., 2017. Vessel segmentation and microaneurysm detection using discriminative dictionary learning and sparse representation. Comput Methods Programs Biomed 139, 93–108. doi:10.1016/j.cmpb.2016.10.015.

Jebaseeli, T., Chelladurai, A., Peter, J., 2019. Retinal blood vessel segmentation from diabetic retinopathy images using tandem pcnn model and deep learning based svm. Optik (Stuttg) 199, 163328. doi:10.1016/j.ijleo.2019.163328.

Jiang, X., Mojon, D., 2003. Adaptive local thresholding by verification-based multithreshold probing with application to vessel detection in retinal images. IEEE Trans. Pattern Anal. Mach. Intell 25 (1), 131—137. doi:10.1109/TPAMI.2003.1159954.

Jiang, Y., Zhang, H., Tan, N., Chen, L., 2019. Automatic retinal blood vessel segmentation based on fully convolutional neural networks. Symmetry (Basel) 11, 1112. doi:10.3390/sym11091112.

Jin, Q., Meng, Z.-P., Pham, T., Chen, Q., Wei, L., Su, R., 2019. Dunet: a deformable network for retinal vessel segmentation. Knowl. Based Syst 178, 149–162.

Kaur, J., Mittal, D., 2017. A generalized method for the detection of vascular structure in pathological retinal images. Biocybernetics and Biomedical Engineering 37. doi:10.1016/j.bbe.2016.09.002.

Khan, K.B., Khaliq, A.A., Jalil, A., Iftikhar, M.A., Ullah, N., Aziz, M.W., Ullah, K., Shahid, M., 2018. A review of retinal blood vessels extraction techniques: challenges, taxonomy, and future trends. Pattern Analysis and Applications 22 (3), 767–802. doi:10.1007/s10044-018-0754-8.

Khan, M., Soomro, T., Khan, T., Bailey, D., Gao, J., Mir, N., 2016. Automatic retinal vessel extraction algorithm based on contrast-sensitive schemes, pp. 1–5. doi:10.1109/IVCNZ.2016.7804441.

Kovács, G., Hajdu, A., 2016. A self-calibrating approach for the segmentation of retinal vessels by template matching and contour reconstruction. Med Image Anal 29(4), 24–46. doi:10.1016/j.media.2015.12.003.

Kumar, D., Pramanik, A., Kar, S.S., Maity, S.P., 2016. Retinal blood vessel segmentation using matched filter and laplacian of gaussian. In: 2016 International Conference on Signal Processing and Communications (SPCOM), pp. 1–5. doi:10.1109/SPCOM.2016.7746666.

Kumar, K., Samal, D., Suraj, 2020. Automated retinal vessel segmentation based on morphological preprocessing and 2d-gabor wavelets. In: Pati, B., Panigrahi, C.R., Buyya, R., Li, K.-C. (Eds.), Advanced Computing and Intelligent Engineering. Springer Singapore, Singapore, pp. 411–423.

Larochelle, H., Bengio, Y., Louradour, J., Lamblin, P., 2009. Exploring strategies for training deep neural networks. Journal of Machine Learning Research 10 (1), 1–40.

Li, Q., Feng, B., Xie, L., Liang, P., Zhang, H., Wang, T., 2016. A cross-modality learning approach for vessel segmentation in retinal images. IEEE Trans Med Imaging 35 (1), 109–118. doi:10.1109/TMI.2015.2457891.

Liskowski, P., Krawiec, K., 2016. Segmenting retinal blood vessels with deep neural networks. IEEE Trans Med Imaging 35 (11), 2369–2380. doi:10.1109/TMI.2016.2546227.

Long, S., Chen, J., Hu, A., Liu, H., Chen, Z., Zheng, D., 2020. Microaneurysms detection in color fundus images using machine learning based on directional local contrast. Biomed Eng Online 19 (1). doi:10.1186/s12938-020-00766-3.

Lupaşcu, C.A., Tegolo, D., Trucco, E., 2010. Fabc: retinal vessel segmentation using adaboost. Trans. Info. Tech. Biomed 14 (5), 1267—1274. doi:10.1109/TITB.2010.2052282.

Lupascu, C.A., Tegolo, D., 2016. A multiscale approach to automatic and unsupervised retinal vessel segmentation using self-organizing maps. In: Proceedings of the 17th International Conference on Computer Systems and Technologies 2016. ACM doi:10.1145/2983468.2983478.

Maier-Hein, L., Eisenmann, M., Reinke, A., Onogur, S., Stankovic, M., Scholz, P., Arbel, T., Bogunovic, H., Bradley, A.P., Carass, A., Feldmann, C., Frangi, A.F., Full, P.M., van Ginneken, B., Hanbury, A., Honauer, K., Kozubek, M., Landman, B.A., März, K., Maier, O., Maier-Hein, K., Menze, B.H., Müller, H., Neher, P.F., Niessen, W., Rajpoot, N., Sharp, G.C., Sirinukunwattana, K., Speidel, S., Stock, C., Stoyanov, D., Taha, A.A., van der Sommen, F., Wang, C.-W., Weber, M.-A., Zheng, G., Jannin, P., Kopp-Schneider, A., 2018. Why rankings of biomedical image analysis competitions should be interpreted with care. Nat Commun 9 (1). doi:10.1038/s41467-018-07619-7.

Mapayi, T., Viriri, S., Tapamo, J.-R., 2015. Adaptive thresholding technique for retinal vessel segmentation based on glcm-energy information. Comput. Math. Methods Medicine 2015, 597475:1–597475:11.

Marin, D., Aquino, A., Gegúndez-Arias, M.E., Bravo, J.M., 2011. A new supervised method for blood vessel segmentation in retinal images by using gray-level and moment invariants-based features. IEEE Trans Med Imaging 30, 146–158.

Martinez-Perez, M.E., Hughes, A.D., Thom, S.A., Bharath, A.A., Parker, K.H., 2007. Segmentation of blood vessels from red-free and fluorescein retinal images. Med Image Anal 11 (1), 47—61. doi:10.1016/j.media.2006.11.004.

Melinscak, M., Prentasic, P., Loncaric, S., 2015. Retinal vessel segmentation using deep neural networks. VISAPP 2015 - 10th International Conference on Computer Vision Theory and Applications; VISIGRAPP, Proceedings 1, 577–582. doi:10.5220/0005313005770582.

Memari, N., Ramli, A.R., Bin Saripan, M.I., Mashohor, S., Moghbel, M., 2017. Supervised retinal vessel segmentation from color fundus images based on matched filtering and adaboost classifier. PLoS ONE 12 (12), 1–35. doi:10.1371/journal.pone.0188939.

Mendonca, A.M., Campilho, A.C., 2006. Segmentation of retinal blood vessels by combining the detection of centerlines and morphological reconstruction. IEEE Trans. Med. Imaging 25 (9), 1200–1213.

Meng, X., Yin, Y., Yang, G., Han, Z., Yan, X., 2015. A framework for retinal vasculature segmentation based on matched filters. Biomed Eng Online 14, 94. doi:10.1186/s12938-015-0089-2.

Miri, M.S., Mahloojifar, A., 2010. Retinal image analysis using curvelet transform and multistructure elements morphology by reconstruction. IEEE Trans Biomed Eng 58, 1183–1192. doi:10.1109/TBME.2010.2097599.

Mo, J., Zhang, L., 2017. Multi-level deep supervised networks for retinal vessel segmentation. Int J Comput Assist Radiol Surg 12. doi:10.1007/s11548-017-1619-0.

Moccia, S., De Momi, E., El Hadji, S., Mattos, L.S., 2018. Blood vessel segmentation algorithms - review of methods, datasets and evaluation metrics. Comput Methods Programs Biomed 158, 71–91. doi:10.1016/j.cmpb.2018.02.001.

Moghimirad, E., Rezatofighi, H., Soltanian-Zadeh, H., 2011. Retinal vessel segmentation using a multi-scale medialness function. Comput. Biol. Med. 42, 50–60. doi:10.1016/j.compbiomed.2011.10.008.

Mookiah, M.R.K., Hogg, S., MacGillivray, T.J., Prathiba, V., Pradeepa, R., Mohan, V., Anjana, R.M., Doney, A.S., Palmer, C.N., Trucco, E., 2021. A review of machine learning methods for retinal blood vessel segmentation and artery/vein classification. Med Image Anal 68, 101905. doi:10.1016/j.media.2020.101905.

Na, T., Xie, J., Zhao, Y., Zhao, Y., Liu, Y., Wang, Y., Liu, J., 2018. Retinal vascular segmentation using superpixel-based line operator and its application to vascular topology estimation. Med Phys 45 (7), 3132–3146. doi:10.1002/mp.12953.

Narkthewan, A., Maneerat, N., 2019. Retina blood vessel detection for diabetic retinopathy diagnosis. In: Proceedings of the 2019 9th International Conference on Biomedical Engineering and Technology. Association for Computing Machinery, New York, NY, USA, pp. 149—152.

Nazari, P., Pourghassem, H., 2013. An automated vessel segmentation algorithm in retinal images using 2d gabor wavelet. In: 2013 8th Iranian Conference on Machine Vision and Image Processing (MVIP). IEEE doi:10.1109/iranianmvip.2013.6779967.

Ngo, L., Han, J., 2017. Multi-level deep neural network for efficient segmentation of blood vessels in fundus images. Electron Lett 53 (16), 1096–1098. doi:10.1049/el.2017.2066.

Niemeijer, M., Staal, J., van Ginneken, B., Loog, M., Abramoff, M. D., 2004. Comparative study of retinal vessel segmentation methods on a new publicly available database. In: Fitzpatrick, J. M., Sonka, M. (Eds.), Medical Imaging 2004: Image Processing. International Society for Optics and Photonics. SPIE, pp. 648–656. doi:10.1117/12.535349.

Noh, K.J., Park, S.J., Lee, S., 2019. Scale-space approximated convolutional neural networks for retinal vessel segmentation. Comput Methods Programs Biomed 178, 237–246. doi:10.1016/j.cmpb.2019.06.030.
Odstrcilik, J., Kolar, R., Budai, A., Hornegger, J., Jan, J., Gazarek, J., Kubena, T., Cernosek, P., Svoboda, O., Angelopoulou, E., 2013. Retinal vessel segmentation by improved matched filtering: evaluation on a new high-resolution fundus image database. IET Image Proc. 7, 373–383. doi:10.1049/iet-ipr.2012.0455.
Palanivel, D.A., Natarajan, S., Gopalakrishnan, S., 2020. Retinal vessel segmentation using multifractal characterization. Appl Soft Comput 94, 106439. doi:10.1016/j.asoc.2020.106439.
Panda, R., Puhan, N.B., Panda, G., 2016. New binary hausdorff symmetry measure based seeded region growing for retinal vessel segmentation. Biocybernetics and Biomedical Engineering 36, 119–129.
Pandey, D., Yin, X., Wang, H., Zhang, Y., 2017. Accurate vessel segmentation using maximum entropy incorporating line detection and phase-preserving denoising. Comput. Vision Image Understanding 155, 162–172. doi:10.1016/j.cviu.2016.12.005.
Park, K.B., Choi, S.H., Lee, J.Y., 2020. M-Gan: retinal blood vessel segmentation by balancing losses through stacked deep fully convolutional networks. IEEE Access 8, 146308–146322. doi:10.1109/ACCESS.2020.3015108.
Porwal, P., Pachade, S., Kokare, M., Deshmukh, G., et al., 2020. IDRiD: diabetic retinopathy – segmentation and grading challenge. Med Image Anal 59, 101561. doi:10.1016/j.media.2019.101561.
Rahebi, J., Hardala, F., 2014. Retinal blood vessel segmentation with neural network by using gray-level co-occurrence matrix-based features. J Med Syst 38, 85. doi:10.1007/s10916-014-0085-2.
Rezaee, K., Haddadnia, J., Tashk, A., 2017. Optimized clinical segmentation of retinal blood vessels by using combination of adaptive filtering, fuzzy entropy and skeletonization. Appl Soft Comput 52, 937–951. doi:10.1016/j.asoc.2016.09.033.
Ricci, E., Perfetti, R., 2007. Retinal blood vessel segmentation using line operators and support vector classification. IEEE Trans Med Imaging 26, 1357–1365.
Roychowdhury, S., Koozekanani, D.D., Parhi, K.K., 2015. Iterative vessel segmentation of fundus images. IEEE Trans. Biomed. Eng. 62 (7), 1738–1749. doi:10.1109/TBME.2015.2403295.
Salazar, A., Kaba, D., Li, Y., Liu, X., 2014. Segmentation of blood vessels and optic disc in retinal images. IEEE J Biomed Health Inform 18. doi:10.1109/JBHI.2014.2302749.
Saleh, D., Eswaran, C., Mueen, A., 2011. An automated blood vessel segmentation algorithm using histogram equalization and automatic threshold selection. Journal of digital imaging : the official journal of the Society for Computer Applications in Radiology 24, 564–572. doi:10.1007/s10278-010-9302-9.
Samuel, P.M., Veeramalai, T., 2019. Multilevel and multiscale deep neural network for retinal blood vessel segmentation. Symmetry (Basel) 11 (7), 946.
Saroj, S.K., Kumar, R., Singh, N.P., 2020. Frchet pdf based matched filter approach for retinal blood vessels segmentation. Comput Methods Programs Biomed 194, 105490. doi:10.1016/j.cmpb.2020.105490.
Shah, S., Tang, T.B., Faye, I., Laude, A., 2017. Blood vessel segmentation in color fundus images based on regional and hessian features. Graefe's Archive for Clinical and Experimental Ophthalmology 255. doi:10.1007/s00417-017-3677-y.
Shukla, A.K., Pandey, R.K., Pachori, R.B., 2020. A fractional filter based efficient algorithm for retinal blood vessel segmentation. Biomed Signal Process Control 59, 101883. doi:10.1016/j.bspc.2020.101883.
Singh, N., Bansal, D., Nagpal, D., 2020. Deep learning based retinal vessel segmentation: a review. Advances in Mathematics: Scientific Journal 9 (6), 3827–3837. doi:10.37418/amsj.9.6.62.
Singh, N.P., Srivastava, R., 2016. Retinal blood vessels segmentation by using gumbel probability distribution function based matched filter. Comput Methods Programs Biomed 129, 40–50. doi:10.1016/j.cmpb.2016.03.001.
Singh, N.P., Srivastava, R., 2017. Weibull probability distribution function-based matched filter approach for retinal blood vessels segmentation. In: Sahana, S.K., Saha, S.K. (Eds.), Advances in Computational Intelligence. Springer Singapore, Singapore, pp. 427–437.
Song, J., Lee, B., 2017. Development of automatic retinal vessel segmentation method in fundus images via convolutional neural networks. In: 2017 39th Annual International Conference of the IEEE Engineering in Medicine and Biology Society (EMBC), pp. 681–684. doi:10.1109/EMBC.2017.8036916.
Soomro, T., Khan, M., Gao, J., Khan, T., Khan, M., Paul, M., 2017. Contrast normalization steps for increased sensitivity of a retinal image segmentation method. Signal Image and Video Processing doi:10.1007/s11760-017-1114-7.
Soomro, T., Khan, T., Khan, M., Gao, J., Paul, M., Zheng, L., 2018. Impact of ica-based image enhancement technique on retinal blood vessels segmentation. IEEE Access PP. doi:10.1109/ACCESS.2018.2794463.
Soomro, T.A., Afifi, A.J., Gao, J., Hellwich, O., Zheng, L., Paul, M., 2019. Strided fully convolutional neural network for boosting the sensitivity of retinal blood vessels segmentation. Expert Syst Appl 134, 36–52. doi:10.1016/j.eswa.2019.05.029.
Sreejini, K., Govindan, V., 2015. Improved multiscale matched filter for retina vessel segmentation using pso algorithm. Egyptian Informatics Journal 16 (3), 253–260. doi:10.1016/j.eij.2015.06.004.
Srinidhi, C.L., Aparna, P., Rajan, J., 2017. Recent advancements in retinal vessel segmentation. J Med Syst 41 (4). doi:10.1007/s10916-017-0719-2.
Staal, J., Abramoff, M., Niemeijer, M., Viergever, M., Ginneken, B., 2004. Ridge-based vessel segmentation in color images of the retina. IEEE Trans Med Imaging 23, 501–559. doi:10.1109/TMI.2004.825627.
Strisciuglio, N., Azzopardi, G., Vento, M., Petkov, N., 2015. Unsupervised delineation of the vessel tree in retinal fundus images doi:10.1201/b19241-26.
Strisciuglio, N., Azzopardi, G., Vento, M., Petkov, N., 2016. Supervised vessel delineation in retinal fundus images with the automatic selection of b-COSFIRE filters. Mach Vis Appl 27 (8), 1137–1149. doi:10.1007/s00138-016-0781-7.
Tamim, N., Elshrkawey, M., Abdel Azim, G., Nassar, H., 2020. Retinal blood vessel segmentation using hybrid features and multi-layer perceptron neural networks. Symmetry (Basel) 12 (6). doi:10.3390/sym12060894.
Tang, Z., Zhang, J., Gui, W., 2017. Selective search and intensity context based retina vessel image segmentation. J Med Syst 41. doi:10.1007/s10916-017-0696-5.
Thangaraj, S., Periyasamy, V., Balaji, R., 2018. Retinal vessel segmentation using neural network. IET Image Proc. 12 (5), 669–678. doi:10.1049/iet-ipr.2017.0284.
Vandewiele, G., Dehaene, I., Kovács, G., Sterckx, L., Janssens, O., Ongenae, F., De Backere, F., De Turck, F., Roelens, K., Decruyenaere, J., Van Hoecke, S., Demeester, T., 2021. Overly optimistic prediction results on imbalanced data: a case study of flaws and benefits when applying over-sampling. Artif Intell Med 111, 101987. doi:10.1016/j.artmed.2020.101987.
Villalobos-Castaldi, F.M., Riverón, E.M.F., Fernández, L., 2010. A fast, efficient and automated method to extract vessels from fundus images. J. Visualization 13, 263–270.
Waheed, A., Akram, M., Khalid, S., Waheed, Z., Khan, M., Shaukat, A., 2015. Hybrid features and mediods classification based robust segmentation of blood vessels. J Med Syst 39. doi:10.1007/s10916-015-0316-1.
Wang, S., Yin, Y., Cao, G., Wei, B., Zheng, Y., Yang, G., 2015. Hierarchical retinal blood vessel segmentation based on feature and ensemble learning. Neurocomputing 149, 708–717. doi:10.1016/j.neucom.2014.07.059.
Wankhede, P.R., Khanchandani, K.B., 2015. Retinal blood vessel segmentation using graph cut analysis. In: 2015 International Conference on Industrial Instrumentation and Control (ICIC), pp. 1429–1432. doi:10.1109/IIC.2015.7150973.
Wu, Y., Xia, Y., Song, Y., Zhang, Y., Cai, W., 2020. Nfn+: a novel network followed network for retinal vessel segmentation. Neural Networks 126. doi:10.1016/j.neunet.2020.02.018.
Xiang, Y., Gao, X., Zou, B., Zhu, C., Qiu, C., Li, X., 2014. Segmentation of retinal blood vessels based on divergence and bot-hat transform. In: 2014 IEEE International Conference on Progress in Informatics and Computing, pp. 316–320. doi:10.1109/PIC.2014.6972349.
Xiuqin, P., Zhang, Q., Zhang, H., Li, S., 2019. A fundus retinal vessels segmentation scheme based on the improved deep learning u-net model. IEEE Access 7, 122634–122643. doi:10.1109/ACCESS.2019.2935138.
Yan, Z., Yang, X., Cheng, K.T., 2018. Joint segment-level and pixel-wise losses for deep learning based retinal vessel segmentation. IEEE Trans. Biomed. Eng. 65 (9), 1912–1923. doi:10.1109/TBME.2018.2828137.
Yang, J., Huang, M., Fu, J., Lou, C., Feng, C., 2020. Frangi based multi-scale level sets for retinal vascular segmentation. Comput Methods Programs Biomed 197, 105752. doi:10.1016/j.cmpb.2020.105752.
You, X., Peng, Q., Yuan, Y., Cheung, Y.-m., Lei, J., 2011. Segmentation of retinal blood vessels using the radial projection and semi-supervised approach. Pattern Recognit 44, 2314–2324. doi:10.1016/j.patcog.2011.01.007.
Yu, C.-Y., Liu, C.-C., Yu, S.-S., 2014. A fovea localization scheme using vessel origin-based parabolic model. Algorithms 7, 456–470. doi:10.3390/a7030456.
Yu, H., Barriga, S., Agurto, C., Zamora, G., Bauman, W., Soliz, P., 2012. Fast vessel segmentation in retinal images using multiscale enhancement and second-order local entropy. Proceedings of SPIE - The International Society for Optical Engineering doi:10.1117/12.911547.
Zhang, B., Zhang, L., Zhang, L., Karray, F., 2010. Retinal vessel extraction by matched filter with first-order derivative of gaussian. Comput. Biol. Med. 40 (4), 438–445. doi:10.1016/j.compbiomed.2010.02.008.
Zhang, J., Dashtbozorg, B., Bekkers, E., Pluim, J.P.W., Duits, R., ter Haar Romeny, B.M., 2016. Robust retinal vessel segmentation via locally adaptive derivative frames in orientation scores. IEEE Trans Med Imaging 35 (12), 2631–2644. doi:10.1109/tmi.2016.2587062.
Zhang, Y., Chung, A.C.S., 2018. Deep Supervision with Additional Labels for Retinal Vessel Segmentation Task. In: Medical Image Computing and Computer Assisted Intervention MICCAI 2018. Springer International Publishing, pp. 83–91. doi:10.1007/978-3-030-00934-2_10.
Zhao, Y., Liu, Y., Wu, X., Harding, S.P., Zheng, Y., 2015. Retinal vessel segmentation: an efficient graph cut approach with retinex and local phase. PLoS ONE 10 (4), e0122332. doi:10.1371/journal.pone.0122332.
Zhao, Y., Rada, L., Chen, K., Harding, S., Zheng, Y., 2015. Automated vessel segmentation using infinite perimeter active contour model with hybrid region information with application to retinal images. IEEE Trans Med Imaging 34, 1797–1807.
Zhou, L., Yu, Q., Xu, X., Gu, Y., Yang, J., 2017. Improving dense conditional random field for retinal vessel segmentation by discriminative feature learning and thin-vessel enhancement. Comput Methods Programs Biomed 148, 13–25. doi:10.1016/j.cmpb.2017.06.016.
Zhu, C., Zou, B., Zhao, R., Cui, J., Duan, X., Chen, Z., Liang, Y., 2017. Retinal vessel segmentation in colour fundus images using extreme learning machine. Computerized Medical Imaging and Graphics 55, 68–77. doi:10.1016/j.compmedimag.2016.05.004. Special Issue on Ophthalmic Medical Image Analysis.